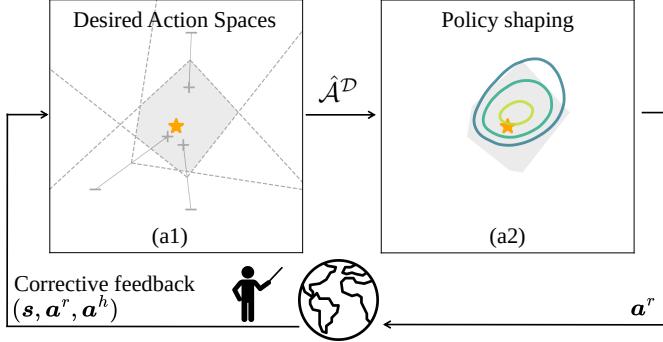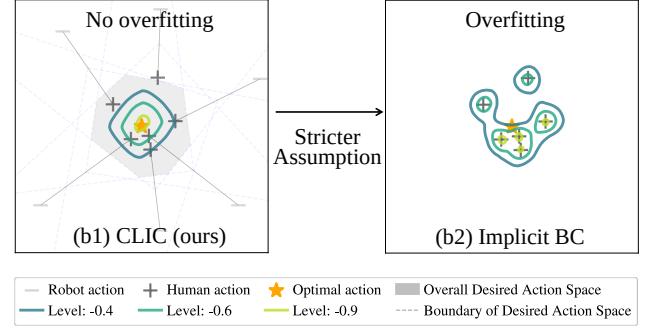# Beyond Behavior Cloning: Robustness through Interactive Imitation and Contrastive Learning

Zhaoting Li, Rodrigo Pérez-Dattari, Robert Babuska, Cosimo Della Santina, Jens Kober

Delft University of Technology, { z.li-23, r.j.perezdattari, r.babuska, c.dellasantina, j.kober }@tudelft.nl

https://clic-webpage.github.io

Fig. 1: A: Our method operates in an Interactive Imitation Learning framework. The robot's policy outputs a robot action $\boldsymbol{a}^r$, which interacts with the environment. The human teacher provides corrective feedback occasionally if the robot action is suboptimal. In (a1), such feedback stored in data buffer $\mathcal{D}$ defines multiple desired action spaces. These regions collectively define an overall desired action space $\hat{\mathcal{A}}^{\mathcal{D}}$. In (a2), the policy, modeled as an energy-based model (EBM), is trained to generate actions within $\hat{\mathcal{A}}^{\mathcal{D}}$. B: Examples of the learned EBMs in a 2D action space. Implicit BC [1] overfits each action label, while our method estimates the optimal action without overfitting.

Abstract—**Behavior cloning (BC) traditionally relies on demonstration data, assuming the demonstrated actions are optimal. This can lead to overfitting under noisy data, particularly when expressive models are used (e.g., the energy-based model in Implicit BC). To address this, we extend behavior cloning into an iterative process of optimal action estimation within the Interactive Imitation Learning framework. Specifically, we introduce *Contrastive policy Learning from Interactive Corrections (CLIC)*. CLIC leverages human corrections to estimate a set of desired actions and optimizes the policy to select actions from this set. We provide theoretical guarantees for the convergence of the desired action set to optimal actions in both single and multiple optimal action cases. Extensive simulation and real-robot experiments validate CLIC's advantages over existing state-of-the-art methods, including stable training of energy-based models, robustness to feedback noise, and adaptability to diverse feedback types beyond demonstrations. Our code will be publicly available soon.**

Index Terms—**Interactive Imitation Learning, Corrective feedback, Contrastive Learning, Learning from Demonstration, Energy-based Models**

I. Introduction

Behavior cloning (BC) enables robots to acquire complex skills simply by imitating human demonstrations [2, 3, 4, 5]. It casts the policy learning problem into a supervised learning framework, under the assumption that human demonstrations are optimal. Implicit BC (IBC) extends BC and achieves better performance in multi-modal tasks, with the policy represented by an energy-based model (EBM). However, IBC suffers from training instability in practice, leading to unreliable results [6, 7]. We identify that the training instability of IBC stems

from an overfitting behavior. This behavior can occur when the policy directly imitates action labels through the *behavior cloning loss*, especially if these labels deviate from the optimal action. Such deviations often arise due to teacher noise or the existence of multiple feasible actions near the optimal one—factors that are common in real-world robot learning tasks. As illustrated in Fig. 1 (b2), an EBM trained via IBC can overfit each noisy action label and deviate from the optimal action, resulting in training instability.

Prior work attempts to address the challenges of implicit policy models by exploring alternative representations, such as diffusion models [6, 8], or flow-based models [9]. While these models often prove more stable during training than EBMs, they do not fundamentally resolve the overfitting issue caused by the BC loss. In fact, although these deep generative models [10, 6, 1] can capture multiple optimal actions in the data, they are also prone to overfitting subtle variations around one optimal action. Consequently, this overfitting issue continues to restrict BC methods to tasks where high-quality demonstration data is available.

In this work, we aim to address this challenge by taking a new perspective that is overlooked in the literature—the loss function and its underlying assumption about the data. To do so, we situate our method within an Interactive Imitation Learning (IIL) framework [11]. In IIL, the human teacher provides demonstrations, also known as absolute corrections or interventions, when the robot actions are suboptimal. Rather than adhering to the standard BC assumption that human actions are always optimal, we adopt a weaker assumption: the

optimal action at a given state can be inferred by aggregating multiple corrective feedback signals. Specifically, we assume that one corrective feedback defines a *desired action space*—a set of actions that could be optimal. We then propose our CLIC method to estimate the potential optimal action, by combining and intersecting multiple desired action spaces defined by the dataset. Concretely, we develop a probabilistic formulation of the desired action space and introduce a Bayesian-inspired loss function that updates the policy to generate actions within the desired space. We use an EBM to represent an implicit policy and also introduce a simplified variant to train an explicit policy.

Beyond demonstration or absolute correction data, our CLIC method can be applied to relative corrections [11, 12, 5]. This feedback indicates the direction of the optimal action relative to the robot's current action but does not specify the distance. From this signal, a suboptimal human action label can be derived and used to update the policy via the BC loss in prior methods [13, 12, 14]. However, imitating suboptimal action labels via the BC loss can lead to incorrect policy updates, and our method addresses this issue by leveraging the desired action space concept, enabling more robust policy learning.

We demonstrate the advantages of our method through a series of experiments. First, our method can train an energy-based model stably, which was believed to be challenging in the literature [6, 7, 15]. Second, our method is able to learn complex multi-modal behavior, thanks to the stable training of energy-based models. Finally, our method can learn from various types of feedback in the action space. Besides typical accurate absolute corrections, it can effectively leverage relative corrections and corrections with noisy or partial information—capabilities that state-of-the-art methods do not offer. This flexibility expands the range of applicable tasks our method can address.

The paper is organized as follows: Section II introduces the related work. Section III shows the preliminaries, including the formulations of IIL, IBC, and our method. Sections IV and V details our CLIC method. Section IV focuses on the construction of the desired action space, and Section V focuses on learning a policy from this desired space. Section VI presents the experimental results in both simulation and the real world. Conclusions are provided in Section VII.

II. RELATED WORK

In this section, we provide an overview of the related work on policy learning from various feedback types, such as demonstration, relative correction, and preference. We also summarize methods for training policies represented by EBMs.

A. Learning from Demonstration

Learning from demonstration aims to teach robot behavior models from demonstration data, which provides the robot with examples of desired actions. Traditional methods often struggled with capturing complex data distributions, especially when multiple optimal actions exist for a given state, such as the task of pushing a T-shape object to a goal configuration [6, 16]. Deep generative models, including EBMs [15, 17],

diffusion models [18, 19], have been introduced to better capture such multi-modal data distributions [10]. EBMs learn unnormalized energy values for inputs and have been applied to learn the energy of the entire state-action space via IBC [1]. Diffusion models, which learn to denoise noise-corrupted data [18, 19], have also been utilized to represent robot policies, resulting in diffusion policies [6, 8]. These policies effectively learn the gradient (score) of the EBM [20] and offer improved training stability [6]. Implicit models, such as EBMs and diffusion policies, have demonstrated superior capability in handling long-horizon, multi-modal tasks compared to explicit policies and have been successfully applied to various real-world applications [21, 22, 10]. These implicit models have been extended into an online interactive imitation learning (IIL) framework [23, 24]. However, as mentioned in the introduction section, the powerful encoding capability of these models can also cause overfitting behavior with behavior cloning loss, especially when the demonstration data deviates from the optimal action. To address this issue while still leveraging their encoding capability, we propose a new perspective on iteratively estimating optimal actions in the IIL framework. Instead of relying on behavior cloning loss, we introduce a novel loss function that updates the policy to align with desired action spaces.

B. Learning from Preference Feedback

Preference-based feedback involves the comparison of different robot trajectory segments. From this, a reward/objective model is usually estimated and employed to obtain a policy [25, 26, 27, 28, 29]. Some approaches enable directly learning a policy by the contrastive learning approach proposed by [30, 31] or direct preference optimization approach [32] to improve efficiency. Moreover, sub-optimal demonstrations can be transformed into preference data to learn a high-quality reward model [33]. Although this feedback modality is promising, it is not very data-efficient. This is because the feedback is given over complete trajectories, requiring the learner to infer per-state behavior and requiring more data and teacher effort. While there are works to make it data efficient via active learning [34] or utilizing prior knowledge of state [35], our paper focuses on human feedback in the state-action space.

C. Learning from Relative Corrective Feedback

Relative corrections provide incremental information on how to improve an action, balancing information richness and simplicity for the teacher [11]. This correction feedback can be transferred into preference data with trajectory pairs and objective functions can be learned from the preference data, as in [26, 36, 37]. Alternatively, [38] proposed directly inferring objective functions without preference transformation. However, these objective functions are linear combinations of features, which may struggle with complex tasks.

Another line of work is the COACH-based framework (Corrective Advice Communicated by Humans), which directly learns a policy from relative corrections [39, 14, 40]. This framework has been extended to utilize the feedback from the state space instead of the action space [41] and combined

with reinforcement learning to increase the RL efficiency[12]. However, COACH-based methods rely on the over-optimistic assumption that the action labels derived from relative corrections are optimal, allowing the policy to be refined by imitating them via the BC loss [13, 12, 14]. This assumption becomes a critical limitation when feedback is aggregated into a reply buffer. As the robot's policy continuously improves, previous feedback may no longer be valid, causing incorrect policy updates [40]. As a result, the buffer size is limited to being small, ensuring it contains only recent corrections. This leads to policies that tend to overfit data collected from recently visited trajectories, making it inefficient compared with demonstration-based methods. In contrast, our CLIC method can utilize the history data, as the desired action spaces created from it will not mislead the policy.

The COACH-based framework utilizes explicit policies[12, 13], limiting its ability to handle multi-modal tasks. Implicit policies, encoded by EBMs, can also be learned using methods like Proxy Value Propagation (PVP)[42]. PVP uses a loss function that only considers the energy values of recorded robot and human actions. As a result, the loss provides limited information and fails to train an EBM effectively. In contrast, our approach generates action samples from the EBM and classifies them into desired and undesired actions based on the desired action space. These classified samples are then used to compute the loss, which can effectively train EBMs.

D. Learning Policies Represented as Energy-Based Models

EBMs have been widely used across different types of feedback data. In reinforcement learning, where data is typically scalar rewards, the energy function is used to encode the action-value function Q, with the relationship $Q_{soft}(\boldsymbol{s}, \boldsymbol{a}) = -\alpha E(\boldsymbol{s}, \boldsymbol{a})$ [43, 44, 45]. Reward-conditioned policies can also be learned through Bayesian approaches [46]. For preference feedback, EBMs can be aligned with human preferences via inverse preference learning [47]. In scenarios involving corrective feedback, where both the robot and the human actions are given, methods such as PVP have been proposed to learn EBMs that assign low energy values to human actions and high energy values to robot actions [42]. For demonstration or absolute correction data, EBMs can be trained directly using the objective that demonstrated actions have lower energy than other actions [48, 1]. In discrete action spaces, EBMs can be straightforward to train [48], though the discrete nature of the action space limits the scope of the method. For continuous action spaces, EBMs can be trained via the InfoNCE loss in IBC [1], through which the energy of human actions is decreased, and the energy of other actions is increased.

Although IBC achieves better performance than explicit policies [1], it is known to suffer from training instability. The process of training EBMs involves selecting counterexample actions, and the quality of these counterexamples significantly impacts the learning outcomes [17, 49]. Empirically, counterexamples that are near data labels are often preferred [50], but these selections may contribute to instability during training [7, 6]. Our method addresses this issue by relaxing the BC assumption and using the proposed desired action space to train EBMs, leading to a stable training process.

III. Preliminaries

A. Interactive Imitation Learning

In a typical Interactive IL (IIL) problem, a Markov Decision Process (MDP) is used to model the decision-making of an agent taught by a human teacher. An MDP is a 5-tuple $(\mathcal{S}, \mathcal{A}, T, R, \gamma)$, where $\mathcal{S}$ represents the set of all possible states in the environment, $\mathcal{A}$ denotes the set of actions the agent can take, $T(\boldsymbol{s}'|\boldsymbol{s}, \boldsymbol{a})$ is the transition probability, $R(\boldsymbol{s}, \boldsymbol{s}', \boldsymbol{a})$ is the reward function, giving the reward received for transitioning from state $\boldsymbol{s}$ to state $\boldsymbol{s}'$ via action $\boldsymbol{a}$, and $\gamma \in [0, 1]$ is the discount factor. The reward typically reflects the desirability of the state transition. A policy in an MDP defines the agent's behavior at a given state, denoted by π. In general, π can be represented by the conditional probability $\pi(\boldsymbol{a}|\boldsymbol{s})$ of the density function $\pi : \mathcal{S} \times \mathcal{A} \to [0, 1]$. Consequently, given a state, π is employed to select an action. The objective in an MDP is to find the optimal policy π^* that maximizes the expected sum of discounted future rewards $J(\pi) = \mathbb{E}\left[\sum_{t=0}^{\infty} \gamma^t R(\boldsymbol{s}_t, \boldsymbol{a}_t)\right]$.

In IIL, a human instructor, known as the *teacher*, aims to improve the behavior of the learning agent, referred to as the *learner*, by providing feedback on the learner's actions. IIL does not rely on a predefined reward function for specific tasks, thanks to the direct guidance provided by the teacher [11]. In this paper, we consider the teacher feedback to act in the state-action space, which is described by the function $\boldsymbol{h} = H(\boldsymbol{s}, \boldsymbol{a})$. The feedback $\boldsymbol{h}$ can be defined according to the feedback type. For instance, in demonstration/intervention feedback, $\boldsymbol{h}$ represents the action the learner should execute at a given state. In contrast, for relative corrective feedback, $\boldsymbol{h}$ is a normalized vector indicating the direction in which the learner's action should be modified, i.e., $\boldsymbol{h} \in \mathcal{H} = \{\boldsymbol{d} \in \mathcal{A} \mid ||\boldsymbol{d}|| = 1\}$. In our context, the reward function is unknown; therefore, we cannot directly maximize the expected accumulated future rewards $J(\pi)$. Instead, an observable surrogate loss, $\ell_\pi(\boldsymbol{s})$, is formulated. This loss measures the alignment of the learner's policy π with the teacher's feedback. In IIL, it is assumed that minimizing $\ell_\pi(\boldsymbol{s})$ indirectly maximizes $J(\pi)$ [51, 11]. As a result, the objective is to determine an optimal learner's policy π^{l*} by solving the following equation:

$$\pi^{l*} = \arg\min_{\pi \in \Pi} \mathbb{E}_{\boldsymbol{s} \sim d_\pi(\boldsymbol{s})}\left[\ell_\pi(\boldsymbol{s})\right] \tag{1}$$

where $d_\pi(\boldsymbol{s})$ is the state distribution induced by the policy π. In practice, the expected value of the surrogate loss in Eq. (1) is approximated using the data collected by a policy that interacts with the environment and the teacher.

B. Implicit Behavior Cloning

Implicit BC (IBC) [1] defines the policy through an energy function $E_\theta(s, a)$ that takes state s and action a as inputs and outputs a scalar energy value. This formulation allows IBC to handle complex, multi-modal, and discontinuous behaviors more effectively than explicit models. The energy function is trained using maximum likelihood estimation by minimizing

the InfoNCE loss [52, 53]:

$$\ell_{\text{InfoNCE}}(\boldsymbol{s}, \boldsymbol{a}, \mathbb{A}^{neg}) = -\log\left[\frac{e^{-E_\theta(\boldsymbol{s},\boldsymbol{a})}}{e^{-E_\theta(\boldsymbol{s},\boldsymbol{a})} + \sum_{j=1}^{N_{\text{neg}}} e^{-E_\theta(\boldsymbol{s},\tilde{\boldsymbol{a}}_j)}}\right], \quad (2)$$

where the action label $\boldsymbol{a}$ is the teacher action, $\tilde{\boldsymbol{a}}_j \in \mathbb{A}^{neg}(j = 1, \ldots, N_{\text{neg}})$ are negative samples, and $\mathbb{A}^{neg}$ is the set that includes negative samples. The InfoNCE loss encourages the model to assign low energy to action labels and high energy to negative samples. To ensure the EBM learns an accurate data distribution, the negative samples should be close to the action label, avoiding overly obvious distinctions that hinder effective learning [49]. This can be achieved by generating negative samples from the current EBM using MCMC sampling with stochastic gradient Langevin dynamics [54, 15]:

$$\tilde{\boldsymbol{a}}_j^i = \tilde{\boldsymbol{a}}_j^{i-1} - \lambda \nabla_{\boldsymbol{a}} E_\theta(\boldsymbol{s}, \tilde{\boldsymbol{a}}_j^{i-1}) + \sqrt{2\lambda}\omega^i, \quad (3)$$

where $\{\tilde{\boldsymbol{a}}_j^0\}$ is initialized using the uniform distribution and ω^i is the standard normal distribution. For each $\tilde{\boldsymbol{a}}_j^0$, we run N_{MCMC} steps of the MCMC chain, with $i = 0, \ldots, N_{\text{MCMC}}$ denoting the step index. The step size $\lambda > 0$ can be adjusted using a polynomially decaying schedule.

During inference, the estimated optimal action $\hat{\boldsymbol{a}}^*$ is obtained by minimizing the energy function, and can be approximated through Langevin MCMC:

$$\hat{\boldsymbol{a}}^* = \arg\min_{\boldsymbol{a}} E_\theta(\boldsymbol{s}, \boldsymbol{a}).$$

One core assumption of IBC is that the action label is optimal and all other actions are not [1]. This assumption simplifies the classification of action samples into positive and negative categories. Specifically, the action label is considered positive, and all other sampled actions are considered negative. However, actions considered as negative may still be valid and should not be overly penalized. This makes selecting appropriate negative samples challenging and introduces instability during the IBC's training process. In contrast, our CLIC method addresses this issue by labeling sampled actions within the desired action space as positive and those outside it as negative, ensuring a more stable and effective training process.

C. Problem Formulation

The objective is to learn a policy π that accurately estimates the optimal action $\boldsymbol{a}^*$ for every state $\boldsymbol{s} \sim d_\pi(\boldsymbol{s})$, using occasional corrective feedback $\boldsymbol{h}$. This feedback is provided by a human teacher in the robot's state-action space, placing the problem in the context of IIL. The feedback $\boldsymbol{h}$ can be either absolute or relative corrections, as defined in Section III-A. Accordingly, the *observed action pair* $(\boldsymbol{a}^r, \boldsymbol{a}^h)$ can be defined, where $\boldsymbol{a}^r$ denotes the robot action and $\boldsymbol{a}^h$ denotes the human feedback action, referred to as human action for simplicity. For absolute correction, we have that $\boldsymbol{a}^h = \boldsymbol{h}$. In contrast, for relative correction, we have that $\boldsymbol{a}^h = \boldsymbol{a}^r + e\boldsymbol{h}$, where the magnitude hyperparameter e is set to a small value.

Although the optimal action may not be directly extracted from human feedback for a given state, it includes information on which subset of $\mathcal{A}$ is more likely to contain optimal actions. Based on this insight, assuming the Euclidean action space $\mathcal{A}$, we introduce the *desired action space* $\hat{\mathcal{A}}(\boldsymbol{a}^r, \boldsymbol{a}^h)$ as the set of desired actions, defined as a function of the observed action

pair $(\boldsymbol{a}^r, \boldsymbol{a}^h)$. Formally, $\hat{\mathcal{A}} : \mathcal{A} \times \mathcal{A} \twoheadrightarrow \mathcal{A}$, where the symbol $\twoheadrightarrow$ defines a set-valued function, i.e., elements of $\mathcal{A} \times \mathcal{A}$ are mapped to subsets of $\mathcal{A}$. Actions within the desired action space are more likely to be optimal than those outside it. The construction of this set is detailed in Section IV.

In this work, we model the policy π using a Deep Neural Network (DNN). To achieve this, following IBC [1], for multi-modal tasks with multiple optimal actions, our policy is defined by the energy function

$$\pi_\theta(\boldsymbol{a}|\boldsymbol{s}) = \frac{\exp(-E_\theta(\boldsymbol{s}, \boldsymbol{a}))}{Z},$$

where Z is a normalizing constant and can be approximated by $Z = \sum_{j=1}^{N_{\text{MCMC}}} \exp(-E_\theta(\boldsymbol{s}, \boldsymbol{a}_j'))$. The samples $\{\boldsymbol{a}_j'\}$ are obtained via Langevin MCMC sampling (see Eq. (3)), and $\boldsymbol{\theta}$ denotes the DNN's parameter vector.

For simpler tasks with a single optimal action for every state, we can consider an explicit Gaussian policy with fixed covariance $\boldsymbol{\Sigma}$ and with mean $\boldsymbol{\mu}_\theta(\boldsymbol{s})$, which we model using a DNN. Hence, we obtain the parameterized policy $\pi_\theta(\boldsymbol{a}|\boldsymbol{s}) \sim \mathcal{N}(\boldsymbol{\mu}_\theta(\boldsymbol{s}), \boldsymbol{\Sigma})$. Both explicit and implicit policies can be estimated using our method based on the desired action space, and we will introduce them in Section V.

IV. DESIRED ACTION SPACE

In this section, we detail how to construct desired action spaces using corrective feedback and show how an overall desired action space, formed jointly by these individual spaces, converges to optimal actions. We begin by outlining the common properties of a general desired action space. Next, we describe the process of constructing the desired action space for two types of feedback: relative and absolute corrections. We then define the overall desired action space and introduce the CLIC algorithm. Finally, we provide theoretical proof of the convergence of the overall desired action space.

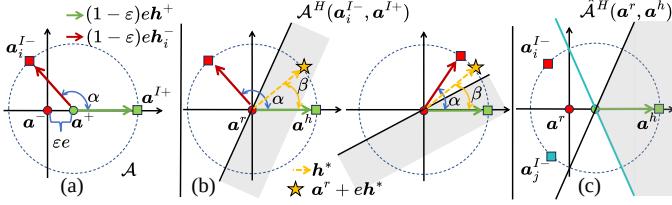### A. General Definition of a Desired Action Space

For a given state, the objective of defining the desired action space is to partition the entire action space into two mutually exclusive categories: desired actions and undesired actions. For an observed action pair $(\boldsymbol{a}^r, \boldsymbol{a}^h)$, we define the *desired action space* $\hat{\mathcal{A}}(\boldsymbol{a}^r, \boldsymbol{a}^h)$ such that the following properties hold:

1) Inclusion of human action; exclusion of robot action:
$$\boldsymbol{a}^h \in \hat{\mathcal{A}}(\boldsymbol{a}^r, \boldsymbol{a}^h) \quad \text{and} \quad \boldsymbol{a}^r \notin \hat{\mathcal{A}}(\boldsymbol{a}^r, \boldsymbol{a}^h).$$

2) Acceptance of suboptimal actions: There may exist other suboptimal actions $\boldsymbol{a}'$ such that:
$$\boldsymbol{a}' \in \hat{\mathcal{A}}(\boldsymbol{a}^r, \boldsymbol{a}^h), \boldsymbol{a}' \neq \boldsymbol{a}^*.$$

To ensure that we can estimate the optimal action by employing the concept of desired action space, we assume that this space includes at least one optimal action $\boldsymbol{a}^*$.

B. Desired Action Space from Relative Corrections

In this section, we detail how to construct desired action spaces from relative corrective feedback. For the observed action pair $(\boldsymbol{a}^r, \boldsymbol{a}^h)$ at state $\boldsymbol{s}$, contrastive action pairs can be obtained. Each of these contrastive action pairs divides the action space in half. By intersecting all the half-spaces, we can

Fig. 2: Illustration of desired action space from relative correction: (a) Generating contrastive action pairs for one observed action pair $(\boldsymbol{a}^r, \boldsymbol{a}^h)$. Squares denote implicit information. (b) Examples of different α for the same $\boldsymbol{h}^*$. With $\varepsilon = 0$, when $\alpha \geq 2\beta$ (left), $\boldsymbol{a} + e\boldsymbol{h}^*$ is inside the desired action space. When $\alpha < 2\beta$ (right), $\boldsymbol{a} + e\boldsymbol{h}^*$ is outside the desired action space. (c) Example of the intersection of the desired half-spaces defined by each contrastive action pair.

obtain the desired action space $\hat{\mathcal{A}}(\boldsymbol{a}^r, \boldsymbol{a}^h)$. We first introduce the definition of the half-space:

1) Desired half-space: Consider a *contrastive action pair* $(\boldsymbol{a}^-, \boldsymbol{a}^+)$ at state $\boldsymbol{s}$, where $\boldsymbol{a}^+$ is referred to as the *positive action* and $\boldsymbol{a}^-$ as the *negative* one. The positive action $\boldsymbol{a}^+$ is defined as a *better* action than $\boldsymbol{a}^-$. Here, *better* indicates that $\boldsymbol{a}^+$ is closer to an optimal action $\boldsymbol{a}^*$ than $\boldsymbol{a}^-$. Formally, the distance of these two actions is defined as $\mathbb{D}(\boldsymbol{a}^+, \boldsymbol{a}^-) = \|\boldsymbol{a}^+ - \boldsymbol{a}^-\|$, and we assume that

$$\mathbb{D}(\boldsymbol{a}^*, \boldsymbol{a}^-) \geq \mathbb{D}(\boldsymbol{a}^*, \boldsymbol{a}^+), \tag{4}$$

From this inequality, the *desired half-space* implied by the action pair $(\boldsymbol{a}^-, \boldsymbol{a}^+)$ can be defined as

$$\mathcal{A}^H(\boldsymbol{a}^-, \boldsymbol{a}^+) = \{\boldsymbol{a} \in \mathcal{A} | \mathbb{D}(\boldsymbol{a}, \boldsymbol{a}^-) \geq \mathbb{D}(\boldsymbol{a}, \boldsymbol{a}^+)\}. \tag{5}$$

The desired half-space satisfies the general definition of desired action space in Section IV-A. Specifically, it is unbounded and includes undesired actions. It also includes the optimal action $\boldsymbol{a}^*$ if Eq. (4) holds.

2) Obtaining contrastive action pairs: In this subsection, we detail how we generate contrastive action pairs $(\boldsymbol{a}^-, \boldsymbol{a}^+)$ from one relative corrective feedback to create desired half-spaces. For the robot action $\boldsymbol{a}^r$ at state $\boldsymbol{s}$, the teacher provides the directional signal $\boldsymbol{h}$ to create one observed action pair $(\boldsymbol{a}^r, \boldsymbol{a}^h)$ (Fig. 2a), where $\boldsymbol{a}^h = \boldsymbol{a}^r + e\boldsymbol{h}$. We introduce the hyperparameter $\varepsilon \in [0, 1)$, which controls how much the robot action gets modified from $\boldsymbol{h}$. Accordingly, we define one contrastive action pair as $(\boldsymbol{a}^-, \boldsymbol{a}^+) = (\boldsymbol{a}^r, \boldsymbol{a}^r + \varepsilon e\boldsymbol{h})$, which are denoted by the red and green circle in Fig. 2a, respectively.

Furthermore, there can be more information contained within relative corrective feedback. This *implicit information* is also utilized, as a way of data augmentation, to exclude some undesired actions in $\mathcal{A}^H(\boldsymbol{a}^r, \boldsymbol{a}^r + \varepsilon e\boldsymbol{h})$. We define the positive correction as $\boldsymbol{h}^+ = \boldsymbol{h}$. Additionally, we define the implicit negative correction $\boldsymbol{h}^-$ as a unit vector that points in a different direction from $\boldsymbol{h}^+$. $\boldsymbol{h}^-$ is sampled from the set:

$$\mathcal{H}^-(\boldsymbol{h}^+, \alpha) = \{\boldsymbol{h}^- \in \mathcal{H} | \; \|\boldsymbol{h}^-\| = 1, \angle(\boldsymbol{h}^-, \boldsymbol{h}^+) = \alpha\},$$

where angle $\alpha \in (0°, 180°]$ is a hyperparameter that indicates how much certainty we have on the directional information provided by the human. There are infinitely many possible $\boldsymbol{h}^-$ if the dimension of $\mathcal{A}$ is greater than 2. In this case, we can sample $\boldsymbol{h}^-$ by generating a unit vector orthogonal to $\boldsymbol{h}^+$ and combining it with $\boldsymbol{h}^+$ at the specified angle α. With sampled $\boldsymbol{h}_i^- \in \mathcal{H}^-$, we can obtain corresponding action

pairs $(\boldsymbol{a}_i^{I-}, \boldsymbol{a}^{I+}), i = 0, \ldots, N_I$, where N_I represents the total number of implicit actions. In Fig. 2a, the green arrow denotes $\boldsymbol{h}^+$ and the red arrow denotes one sample of $\boldsymbol{h}^-$. The action pairs $(\boldsymbol{a}_i^{I-}, \boldsymbol{a}^{I+})$ are defined as follows, illustrated by the squares in Fig. 2a:

$$\boldsymbol{a}^{I+} = \boldsymbol{a}^h, \boldsymbol{a}_i^{I-} = \boldsymbol{a}^r + \varepsilon e\boldsymbol{h}^+ + (1 - \varepsilon)e\boldsymbol{h}_i^-.$$

3) Desired action space by combining implicit desired half-spaces: Since the desired half-space defined by each contrastive action pair is convex and includes the human action, their intersection results in a non-empty combined space. This combined space also has a smaller volume compared to each individual half-space. As a result, for one relative corrective feedback, we define the *desired action space* $\hat{\mathcal{A}}^H(\boldsymbol{a}^r, \boldsymbol{a}^h)$ as the intersection of the desired half-spaces enforced by each contrastive action pair $(\boldsymbol{a}_i^{I-}, \boldsymbol{a}^{I+})$:

$$\hat{\mathcal{A}}^H(\boldsymbol{a}^r, \boldsymbol{a}^h) = \bigcap_{i=0}^{N_I} \mathcal{A}^H(\boldsymbol{a}_i^{I-}, \boldsymbol{a}^{I+}). \tag{6}$$

One example of the desired action space in a 2D action space is shown in Fig. 2c. Importantly, to exclude some undesired actions in $\mathcal{A}^H(\boldsymbol{a}^r, \boldsymbol{a}^r + \varepsilon e\boldsymbol{h})$ while ensuring $\boldsymbol{a}^*$ remains within $\hat{\mathcal{A}}^H(\boldsymbol{a}^r, \boldsymbol{a}^h)$, the hyperparameter α and ε need careful selection. If α is too small, $\hat{\mathcal{A}}^H(\boldsymbol{a}^r, \boldsymbol{a}^h)$ may fail to include $\boldsymbol{a}^*$, as illustrated in Fig. 2b. Similarly, if ε is set too large, it could also exclude $\boldsymbol{a}^*$ from the desired space.

C. Desired Action Space from Demonstration Feedback

In Section IV-B, we described constructing the desired action space using relative corrective feedback. Similarly, the desired action space can be constructed from demonstrations or absolute corrections. We introduce two methods to achieve this. One approach transforms demonstration data into relative corrections. Alternatively, a stricter assumption can be made by defining a circular desired action space centered around the demonstrated actions. These two methods are detailed below:

1) Treating demonstration as relative correction: For the robot action $\boldsymbol{a}^r$ at state $\boldsymbol{s}$, if the feedback received is demonstration $\boldsymbol{a}^h$, one way to utilize the desired action space $\hat{\mathcal{A}}^H(\boldsymbol{a}^r, \boldsymbol{a}^h)$ defined in Section IV-B is to transform the demonstration data into relative corrective data. The directional signal is obtained as $\boldsymbol{h} = (\boldsymbol{a}^h - \boldsymbol{a}^r)/e$. Here, instead of being a hyperparameter, the correction magnitude e is known as the distance between the robot action and human action: $e = \|\boldsymbol{a}^h - \boldsymbol{a}^r\|$.

2) Circular desired action space: Besides the unbounded desired action space $\hat{\mathcal{A}}^H(\boldsymbol{a}^r, \boldsymbol{a}^h)$, we can make stricter assumptions by redefining the desired action space concept. This allows us to leverage additional information from the demonstration data. Specifically, the *circular desired action space* defined by the demonstration data can be

$$\hat{\mathcal{A}}^C(\boldsymbol{a}^r, \boldsymbol{a}^h) = \{\boldsymbol{a} \in \mathcal{A} | (1 - \varepsilon) \cdot \mathbb{D}(\boldsymbol{a}^h, \boldsymbol{a}^r) \geq \mathbb{D}(\boldsymbol{a}, \boldsymbol{a}^h)\}, \tag{7}$$

which is the ball centered at $\boldsymbol{a}^h$ with radius $(1-\varepsilon) \cdot \mathbb{D}(\boldsymbol{a}^h, \boldsymbol{a}^r)$. The hyperparameter $\varepsilon \in [0, 1)$ adjusts the radius of the ball. For $\varepsilon \to 1$, the ball reduces to one action point $\boldsymbol{a}^h$. By this definition, we assume the optimal action is within the ball, and all the actions within the ball are potential candidates of the optimal action. If the feedback consists only of the teacher

Algorithm 1 CLIC Algorithm

Require: buffer $\mathcal{D}$, update frequency b
1: **for** episode = 1, 2, . . . **do**
2:     **for** $t = 1, 2, \ldots$ **do**
3:         Observe $\boldsymbol{s}_t$, execute $\boldsymbol{a}_t^r$
4:         Receive feedback $\boldsymbol{a}_t^h$ for $\boldsymbol{a}_t^r$, if $\boldsymbol{a}_t^r$ is suboptimal
5:         Append $[\boldsymbol{s}_t, \boldsymbol{a}_t^r, \boldsymbol{a}_t^h]$ to $\mathcal{D}$, if $\boldsymbol{a}_t^h$ is provided
6:         **if** $t\%b = 0$ or $\boldsymbol{a}_t^h$ is provided **then**
7:             Sample batch $\mathcal{B}$ from $\mathcal{D}$
8:             Obtain desired action spaces (Sec. IV-B, IV-C)
9:             Update policy $\pi_{\boldsymbol{\theta}}$ (Algorithm 2, Sec. V)
10:        **end if**
11:     **end for**
12:     Update policy $\pi_{\boldsymbol{\theta}}$ as line 7-9 for N_{training} steps
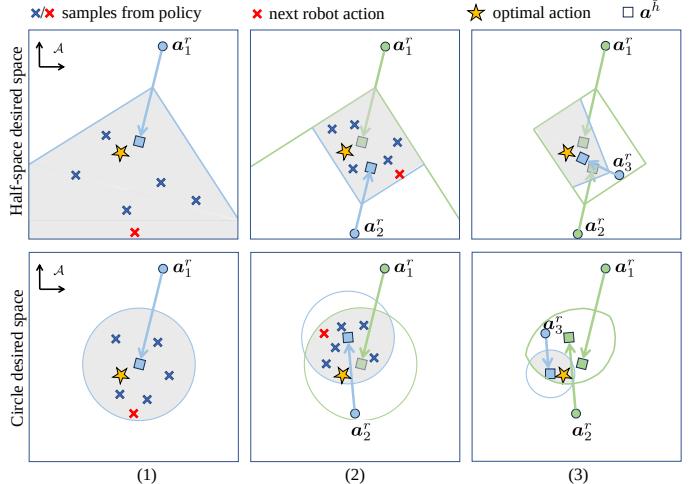13: **end for**

---

action and the robot action is unavailable, we can introduce a hyperparameter r to define the radius. However, tuning r can be challenging. A small value of r could reduce CLIC into IBC, as shown in an experiment in Section VI-C, and a large value of r could hinder convergence.

To differentiate between the desired action spaces constructed in different ways, we refer to the CLIC method using a circular desired action space $\hat{\mathcal{A}}^C(\boldsymbol{a}^r, \boldsymbol{a}^h)$ as *CLIC-Circular*. And *CLIC-Half* refers to the method that uses the half-space desired action space $\hat{\mathcal{A}}^H(\boldsymbol{a}^r, \boldsymbol{a}^h)$, which is defined by intersecting desired half-spaces.

D. CLIC Algorithm and Overall Desired Action Space

The desired action space $\hat{\mathcal{A}}(\boldsymbol{a}^r, \boldsymbol{a}^h)$, resulting from a single corrective feedback, includes the optimal action but also other undesired actions. By incorporating multiple feedback inputs, the desired action spaces from these inputs can collectively define an *overall desired action space* for each state. CLIC is designed with the idea of aggregating multiple corrections: every time new feedback input is received for a given state, the overall desired action space for that state gets refined (see Fig. 3). This fits seamlessly with the IIL framework, where the teacher provides feedback when the robot performs suboptimally. We first introduce the CLIC algorithm in Section IV-D1 to provide a high-level overview, then elaborate on the overall desired action space and its convergence in Section IV-D2.

1) Algorithm of CLIC: Algorithm 1 presents our CLIC method within the IIL framework, shaping the learner's policy through multiple corrections. We assume the existence of a policy update mechanism at this stage, with details deferred to Section V. We define the data buffer as $\mathcal{D} = \{[\boldsymbol{s}_t, \boldsymbol{a}_t^r, \boldsymbol{a}_t^h], t = 1, \ldots\}$, which contains all the corrective feedback received (line 5). The core part of this algorithm is from line 7 to 9. In line 7, a batch of data $\mathcal{B}$ is sampled from the buffer $\mathcal{D}$. If new data is available, it is included in $\mathcal{B}$ to ensure the robot quickly adapts to the teacher's instructions. In line 8, the desired action spaces are generated for each feedback signal in the sampled buffer. Line 9 calculates the loss based on the desired action space to update the policy $\pi_{\boldsymbol{\theta}}$ (this loss will be introduced in Section V). At the end of each episode, the policy is updated for N_{training} training steps (line 12).

Fig. 3: Overall desired action space obtained from multiple feedback inputs within one state. (1) A human action $\boldsymbol{a}_1^h$ is provided, forming an inital overall desired action space $\hat{\mathcal{A}}_1^{\mathcal{D}(\boldsymbol{s})} = \hat{\mathcal{A}}(\boldsymbol{a}_1^r, \boldsymbol{a}_1^h)$. The robot policy is updated to generate actions within this space. (2) $\boldsymbol{a}_2^r$ is selected, and the human feedback $\boldsymbol{a}_2^h$ is provided, shrinking the overall desired space to $\hat{\mathcal{A}}_2^{\mathcal{D}(\boldsymbol{s})}$. The policy is then updated accordingly. (3) The process continues with further feedback (e.g., $\boldsymbol{a}_3^h$), leading to a smaller overall desired space $\hat{\mathcal{A}}_3^{\mathcal{D}(\boldsymbol{s})}$.

2) Overall desired action space: Formally, we denote the feedback received at state $\boldsymbol{s}$ by $\mathcal{D}(\boldsymbol{s}) = \{[\boldsymbol{s}, \boldsymbol{a}_i^r, \boldsymbol{a}_i^h], i = 1, \ldots, k\}$, where k indicates the number of feedback samples. We denote the *overall desired action space* enforced by $\mathcal{D}(\boldsymbol{s})$ as $\hat{\mathcal{A}}_k^{\mathcal{D}(\boldsymbol{s})}$. Define the set of optimal actions at state $\boldsymbol{s}$ as $\mathcal{A}^*(\boldsymbol{s}) = \{\boldsymbol{a}_i^*, i = 1, \ldots, N_*\}$, where N_* is the number of optimal actions at state $\boldsymbol{s}$. If $N_* = 1$ at state $\boldsymbol{s}$, $\hat{\mathcal{A}}_k^{\mathcal{D}(\boldsymbol{s})} = \cap_i^k \hat{\mathcal{A}}(\boldsymbol{a}_i^r, \boldsymbol{a}_i^h)$. For the general multiple optimal actions case ($N_* > 1$), we define

$$\hat{\mathcal{A}}_k^{\mathcal{D}(\boldsymbol{s})} = \begin{cases} \hat{\mathcal{A}}_{k-1}^{\mathcal{D}(\boldsymbol{s})} \cap \hat{\mathcal{A}}(\boldsymbol{a}_k^r, \boldsymbol{a}_k^h), \text{if } \hat{\mathcal{A}}_{k-1}^{\mathcal{D}(\boldsymbol{s})} \cap \hat{\mathcal{A}}(\boldsymbol{a}_k^r, \boldsymbol{a}_k^h) \neq \varnothing & (8) \\ \hat{\mathcal{A}}_{k-1}^{\mathcal{D}(\boldsymbol{s})} \cup \hat{\mathcal{A}}(\boldsymbol{a}_k^r, \boldsymbol{a}_k^h), \text{otherwise} & (9) \end{cases}$$

We then provide a theoretical guarantee that as $k \to \infty$, $\hat{\mathcal{A}}_k^{\mathcal{D}(\boldsymbol{s})}$ converges to optimal actions:

Proposition 1: For any state $\boldsymbol{s}$, assume a trained policy $\pi_{\boldsymbol{\theta}}$ always select actions from $\hat{\mathcal{A}}_k^{\mathcal{D}(\boldsymbol{s})}$, and there are a finite number of optimal actions. Assume that there is a nonzero probability for the teacher to provide feedback to each suboptimal action $\boldsymbol{a}_{k+1}^r \sim \pi_{\boldsymbol{\theta}}(\cdot|\boldsymbol{s})$. Then, as $k \to \infty$, $\hat{\mathcal{A}}_k^{\mathcal{D}(\boldsymbol{s})}$ converges to $\mathcal{A}^*(\boldsymbol{s})$ or a subset of $\mathcal{A}^*(\boldsymbol{s})$.

Proof: In Appendix VIII-A. ∎

Fig. 3 illustrates the convergence process for both the half-space and circular desired action spaces. Beginning with an initial set $\mathcal{A}_{k-1}^{\mathcal{D}(\boldsymbol{s})}$, the robot samples actions from the policy and selects one action, denoted as $\boldsymbol{a}_k^r$. According to the assumption stated in Proposition 1, $\boldsymbol{a}_k^r \in \mathcal{A}_{k-1}^{\mathcal{D}(\boldsymbol{s})}$. The teacher will provide new feedback $\boldsymbol{a}_k^h$ if $\boldsymbol{a}_k^r$ is suboptimal. For a single optimal action case, the observed action pair $(\boldsymbol{a}_k^r, \boldsymbol{a}_k^h)$ leads to a reduction in the volume of the overall desired action space (Eq. (8)). With an infinite amount of feedback, $\mathcal{A}_k^{\mathcal{D}(\boldsymbol{s})}$ converges to the optimal action $\boldsymbol{a}^*$. When multiple optimal actions exist, the difference is that $\mathcal{A}_k^{\mathcal{D}(\boldsymbol{s})}$ can also

expand its volume (Eq. (9)). Nevertheless, because only a finite number of optimal actions exists, the volume of $\mathcal{A}_k^{\mathcal{D}(s)}$ cannot increase indefinitely. Instead, its volume ultimately decreases and converges to $\mathcal{A}^*(s)$ or a subset of $\mathcal{A}^*(s)$ given an infinite amount of feedback. In practice, for continuous state-action spaces, it is unlikely to receive multiple feedback inputs for the exact same state. Therefore, we assume that for similar states, the generalization capabilities of DNNs allow for this process of aggregating multiple feedback signals.

V. POLICY SHAPING VIA DESIRED ACTION SPACES

In this section, we show how to train a policy using desired action spaces. First, Section V-A outlines the algorithm for implicit policy shaping, providing an overview of its key components. Next, in Section V-B, we introduce a probabilistic formulation of the desired action space. This formulation defines an observation model of how an action can explain the observed action pair. Based on this model, we derive a posterior distribution, which serves as a target for updating the robot's policy. Then, based on this idea, in Section V-C, we present a novel loss function used to train an implicit policy, represented by an energy-based model. Finally, in Section V-D, we provide a simplified formulation, which assumes a Gaussian-parameterized policy. This formulation can be useful for simpler tasks, where data efficiency is more critical than policy complexity.

A. Algorithm for Implicit Policy Shaping

The algorithm for training the implicit policy, represented as an EBM, is outlined in Algorithm 2. This algorithm leverages a novel loss function (line 2-5), which will be detailed in the following sections, to effectively shape the policy and align it with desired action spaces. In each update step, action samples are drawn from the current EBM using MCMC sampling (line 1). These sampled actions are then used to estimate both the current policy distribution and the target policy distribution (lines 2- 4). Finally, the KL loss is computed based on these estimates, and the EBM parameters $\boldsymbol{\theta}$ are updated accordingly (line 5). An example of the training process using Algorithm 2 is shown in Fig. 4, which illustrates how the algorithm adjusts the density of an EBM and effectively aligns it with a desired action space.
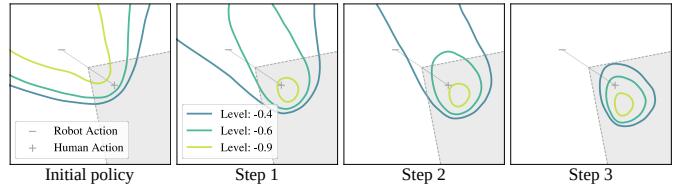

Algorithm 2 Implicit Policy shaping

Require: Buffer batch $\mathcal{B}$, energy-based model $E_{\boldsymbol{\theta}}$
1: Generate action samples $\mathbb{A}$ from $E_{\boldsymbol{\theta}}(\boldsymbol{s}, \cdot), \boldsymbol{s} \in \mathcal{B}$
2: Estimate policy $\pi_{\boldsymbol{\theta}}(\boldsymbol{a}|\boldsymbol{s}) \propto \exp(-E_{\boldsymbol{\theta}}(\boldsymbol{s}, \boldsymbol{a})), \boldsymbol{a} \in \mathbb{A}$
3: Calculate observation model $p(\boldsymbol{a}^h \succeq \boldsymbol{a}^r | \boldsymbol{a}, \boldsymbol{s}), \boldsymbol{a} \in \mathbb{A}$
4: Estimate target distribution $\pi^{\text{target}}(\boldsymbol{a}|\boldsymbol{s}), \boldsymbol{a} \in \mathbb{A}$
5: Calculate KL loss $\mathbb{E}_{\mathcal{B}}\left[\text{KL}\left(\pi^{\text{target}}(\boldsymbol{a}|\boldsymbol{s})\|\pi_{\boldsymbol{\theta}}(\boldsymbol{a}|\boldsymbol{s})\right)\right]$

B. Probabilistic Modeling of Desired Action Spaces

Our objective is to infer the optimal action from multiple desired action spaces. To do so, we seek to define a probability (or utility) function that measures how likely any given random

Fig. 4: 2D example of the training process of the energy-based model using Algorithm 2. The gray-shaped area represents the desired action space enforced by the observed action pair. The contour map shows the value of the EBM. In this example, the batch size is set to 1, and the same observed action pair $(\boldsymbol{a}^r, \boldsymbol{a}^h)$ is used to update the EBM over three consecutive steps. Initially, the EBM has the most density outside the desired action space $\hat{\mathcal{A}}(\boldsymbol{a}^r, \boldsymbol{a}^h)$. After the first update step, the peak density shifts toward the desired action space but still retains significant density outside it. With two additional update steps, the EBM is fully inside the desired action space.

action is to be optimal, conditioned on the information of a desired action space. As a first step, we introduce the observation model $\Pr[\boldsymbol{a} \in \hat{\mathcal{A}}(\boldsymbol{a}^r, \boldsymbol{a}^h)|\boldsymbol{a}, \boldsymbol{s}]$. This model outputs the probability of a given action $\boldsymbol{a}$ belonging to set $\hat{\mathcal{A}}(\boldsymbol{a}^r, \boldsymbol{a}^h)$, conditioned on state $\boldsymbol{s}$.

1) Observation model for CLIC-Half: For $\hat{\mathcal{A}}(\boldsymbol{a}^r, \boldsymbol{a}^h)$ defined by the intersection of desired half-spaces in Eq. (6), by leveraging conditional independence, we have

$$\Pr[\boldsymbol{a} \in \hat{\mathcal{A}}(\boldsymbol{a}^r, \boldsymbol{a}^h)|\boldsymbol{a}, \boldsymbol{s}] = \prod_{i=1}^{N_I} \Pr[\boldsymbol{a} \in \mathcal{A}^H(\boldsymbol{a}_i^-, \boldsymbol{a}_i^+)|\boldsymbol{a}, \boldsymbol{s}],$$

where $(\boldsymbol{a}_i^-, \boldsymbol{a}_i^+)$ are the contrastive action pairs obtained from the observed action pair $(\boldsymbol{a}^r, \boldsymbol{a}^h)$, as explained in Section IV-B2. The observation model of one desired half-space $\mathcal{A}^H(\boldsymbol{a}^-, \boldsymbol{a}^+)$ is defined as:

$$\Pr[\boldsymbol{a} \in \mathcal{A}^H(\boldsymbol{a}^-, \boldsymbol{a}^+)|\boldsymbol{a}, \boldsymbol{s}] = \begin{cases} 1, \|\boldsymbol{a} - \boldsymbol{a}^-\| - \|\boldsymbol{a} - \boldsymbol{a}^+\| \geq 0 \\ 0, \|\boldsymbol{a} - \boldsymbol{a}^-\| - \|\boldsymbol{a} - \boldsymbol{a}^+\| < 0 \end{cases}$$
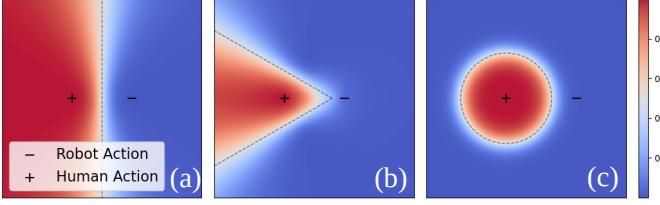
The above observation model outputs 1 if the given action lies within the desired half-space, as defined by Eq. (5), and 0 otherwise. To account for the potential noise in human feedback and the possible violation of underlying assumptions in real-world scenarios, the hard decision boundary can be smoothed by a sigmoid function:

$$\Pr[\boldsymbol{a} \in \mathcal{A}^H(\boldsymbol{a}^-, \boldsymbol{a}^+)|\boldsymbol{a}, \boldsymbol{s}] = \sigma_T(\|\boldsymbol{a} - \boldsymbol{a}^-\| - \|\boldsymbol{a} - \boldsymbol{a}^+\|) \quad (10)$$

where $\sigma_T(x) = \frac{1}{1+\exp(-x/T)}$ is the sigmoid function and $T > 0$ is a temperature parameter that determines how sharply the function transitions between 0 and 1. As $T \to 0$, $\sigma_T(x)$ behaves more like a step function: the probability becomes 1 if $\boldsymbol{a}$ is inside $\mathcal{A}^H(\boldsymbol{a}^-, \boldsymbol{a}^+)$ and 0 otherwise. One example of the observation model of the desired half-space in 2D is shown in Fig. 5(a). Similarly, Fig. 5(b) provides an example of the observation model for the desired action space $\hat{\mathcal{A}}(\boldsymbol{a}^r, \boldsymbol{a}^h)$, which is the intersection of multiple desired half-spaces.

2) Observation model for CLIC-Circular: As introduced in Section IV-C, the desired action space can be more restricted if the feedback is demonstration data. In this case, similar to the way that we define Eq. (10), the observation model for the circular desired action space is defined as:

$$\Pr[\boldsymbol{a} \in \hat{\mathcal{A}}(\boldsymbol{a}^r, \boldsymbol{a}^h)|\boldsymbol{a}, \boldsymbol{s}] = \sigma_T(r(\boldsymbol{a}^r, \boldsymbol{a}^h) - \|\boldsymbol{a} - \boldsymbol{a}^h\|),$$

Fig. 5: Illustration of the observation model $\Pr[\boldsymbol{a} \in \hat{\mathcal{A}}(\boldsymbol{a}^r, \boldsymbol{a}^h)|\boldsymbol{a}, \boldsymbol{s}]$ for all $\boldsymbol{a} \in \mathcal{A}$. In each figure, the state $\boldsymbol{s}$, human action $\boldsymbol{a}^h$, and robot action $\boldsymbol{a}^r$ are fixed, while the action $\boldsymbol{a}$ varies across the action space. The black dotted line denotes the boundary of $\hat{\mathcal{A}}(\boldsymbol{a}^r, \boldsymbol{a}^h)$, which is smoothed by a sigmoid function. (a) Desired half-space; (b) Desired action space from relative correction; (c) Circular desired action space.

where $r(\boldsymbol{a}^r, \boldsymbol{a}^h) = (1 - \varepsilon)\|\boldsymbol{a}^h - \boldsymbol{a}^r\|$ is the radius of the circular desired action space, as in Eq. (7). The temperature T controls the steepness of the sigmoid function, for $T \to 0$, the probability becomes 1 for all action inside the ball defined by $r(\boldsymbol{a}^r, \boldsymbol{a}^h)$, and 0 otherwise.

3) Posterior distribution of desired actions: The observation model $\Pr[\boldsymbol{a} \in \hat{\mathcal{A}}(\boldsymbol{a}^r, \boldsymbol{a}^h)|\boldsymbol{a}, \boldsymbol{s}]$ indicates how likely a given action $\boldsymbol{a}$ can explain the observed action pair $(\boldsymbol{a}^r, \boldsymbol{a}^h)$ and also how likely it belongs to the corresponding desired action space $\mathcal{A}(\boldsymbol{a}^r, \boldsymbol{a}^h)$. For simplicity, we use $\boldsymbol{a}^h \succeq \boldsymbol{a}^r$ to indicate that $\boldsymbol{a} \in \hat{\mathcal{A}}(\boldsymbol{a}^r, \boldsymbol{a}^h)$. This notation $\boldsymbol{a}^h \succeq \boldsymbol{a}^r$ indicates that an action $\boldsymbol{a}$ is considered to be within the set $\hat{\mathcal{A}}(\boldsymbol{a}^r, \boldsymbol{a}^h)$, defined by the condition that $\boldsymbol{a}^h$ is more preferred than $\boldsymbol{a}^r$ by the human teacher. We then rewrite the observation model as $p(\boldsymbol{a}^h \succeq \boldsymbol{a}^r|\boldsymbol{a}, \boldsymbol{s})$.

Furthermore, we define the prior distribution $p(\boldsymbol{a}|\boldsymbol{s})$ as the probability of selecting action $\boldsymbol{a}$ given state $\boldsymbol{s}$. This distribution represents the initial belief about the likelihood of selecting actions before incorporating any new observed action pairs. By the Bayes' rule, the posterior belief $p(\boldsymbol{a}|\boldsymbol{a}^h \succeq \boldsymbol{a}^r, \boldsymbol{s})$ can be obtained as

$$p(\boldsymbol{a}|\boldsymbol{a}^h \succeq \boldsymbol{a}^r, \boldsymbol{s}) = \frac{p(\boldsymbol{a}^h \succeq \boldsymbol{a}^r|\boldsymbol{a}, \boldsymbol{s})p(\boldsymbol{a}|\boldsymbol{s})}{p(\boldsymbol{a}^h \succeq \boldsymbol{a}^r|\boldsymbol{s})}, \quad (11)$$

where $p(\boldsymbol{a}^h \succeq \boldsymbol{a}^r|\boldsymbol{s}) = \int_{\boldsymbol{a}'} p(\boldsymbol{a}^h \succeq \boldsymbol{a}^r|\boldsymbol{a}', \boldsymbol{s})p(\boldsymbol{a}'|\boldsymbol{s})d\boldsymbol{a}'$ is the normalization term. The posterior $p(\boldsymbol{a}|\boldsymbol{a}^h \succeq \boldsymbol{a}^r, \boldsymbol{s})$ represents the probability of $\boldsymbol{a}$ being selected, given the observed action pair $(\boldsymbol{a}^r, \boldsymbol{a}^h)$ at state $\boldsymbol{s}$. This posterior can be used to estimate optimal actions thanks to the definition of the desired action space. Specifically, the desired action space $\hat{\mathcal{A}}(\boldsymbol{a}^r, \boldsymbol{a}^h)$ is defined to include actions that could potentially be the optimal actions, while actions outside this space are considered undesirable. As a result, the posterior $p(\boldsymbol{a}|\boldsymbol{a}^h \succeq \boldsymbol{a}^r, \boldsymbol{s})$ indicates the likelihood that $\boldsymbol{a}$ is an optimal action, given the observed data. Therefore, a natural way of learning a policy from data $(\boldsymbol{s}, \boldsymbol{a}^r, \boldsymbol{a}^h)$ is to align it with this posterior distribution, as we will detail in the following section.

C. Loss function for Implicit Policy Shaping

The desired action space constructed by the observed action pair can be utilized to shape the robot's policy. The intuition is that at a given state $\boldsymbol{s}$, one observed action pair $(\boldsymbol{a}^r, \boldsymbol{a}^h)$ indicates that the policy $\pi_{\boldsymbol{\theta}}$ should increase the probability of selecting actions within the set $\hat{\mathcal{A}}(\boldsymbol{a}^r, \boldsymbol{a}^h)$, denoted

as $\pi_{\boldsymbol{\theta}}(\boldsymbol{a} \in \hat{\mathcal{A}}(\boldsymbol{a}^r, \boldsymbol{a}^h)|\boldsymbol{s})$. Consequently, the probability of selecting actions outside this set, $\pi_{\boldsymbol{\theta}}(\boldsymbol{a} \notin \hat{\mathcal{A}}(\boldsymbol{a}^r, \boldsymbol{a}^h)|\boldsymbol{s})$, should decrease. To increase $\pi_{\boldsymbol{\theta}}(\boldsymbol{a} \in \hat{\mathcal{A}}(\boldsymbol{a}^r, \boldsymbol{a}^h)|\boldsymbol{s})$, the policy $\pi_{\boldsymbol{\theta}}$ can be updated to align with a target distribution that assigns a high probability to actions within $\hat{\mathcal{A}}(\boldsymbol{a}^r, \boldsymbol{a}^h)$. The posterior distribution defined in Section V-B can be this target distribution $\pi^{\text{target}}(\boldsymbol{a}|\boldsymbol{s}) := p(\boldsymbol{a}|\boldsymbol{a}^h \succeq \boldsymbol{a}^r, \boldsymbol{s})$. As a result, the policy can then be optimized by minimizing the KL divergence between the estimated posterior and the policy distribution:

$$\ell_{KL}(\boldsymbol{\theta}) = \mathop{\mathbb{E}}_{(\boldsymbol{a}^h, \boldsymbol{a}^r, \boldsymbol{s}) \sim p_{\mathcal{D}}} \left[\text{KL}\left(\pi^{\text{target}}(\boldsymbol{a}|\boldsymbol{s}) \big\| \pi_{\boldsymbol{\theta}}(\boldsymbol{a}|\boldsymbol{s}) \right) \right] \quad (12)$$

To calculate the above loss, we need to evaluate the posterior distribution $p(\boldsymbol{a}|\boldsymbol{a}^h \succeq \boldsymbol{a}^r, \boldsymbol{s})$. This posterior depends on the prior distribution $p(\boldsymbol{a}|\boldsymbol{s})$, which has yet to be specified. In the following sections, we introduce two different assumptions for this prior distribution.

1) Uniform Bayes loss: We assume a uniform distribution of $p(\boldsymbol{a}|\boldsymbol{s})$, then the posterior distribution is directly proportional to the prior distribution:

$$\pi^{\text{target}}(\boldsymbol{a}|\boldsymbol{s}) \propto p(\boldsymbol{a}^h \succeq \boldsymbol{a}^r|\boldsymbol{a}, \boldsymbol{s}).$$

To approximate the loss in Eq. (12), we estimate both $\pi^{\text{target}}(\boldsymbol{a}|\boldsymbol{s})$ and $\pi_{\boldsymbol{\theta}}(\boldsymbol{a}|\boldsymbol{s})$ using a set of action samples, defined as follows:

$$\mathbb{A} = \{\boldsymbol{a}^h, \boldsymbol{a}^r\} \cup \{\boldsymbol{a}_j | j = 1, \dots, N_a\},$$

where N_a samples $\{\boldsymbol{a}_j\}$ can be obtained by Langevin MCMC as described in Eq. (3). Given this set of actions $\mathbb{A}$, the policy evaluated at each sampled action can be approximated via

$$\pi_{\boldsymbol{\theta}}(\boldsymbol{a}|\boldsymbol{s}) = \frac{e^{-E_{\boldsymbol{\theta}}(\boldsymbol{s}, \boldsymbol{a})}}{\sum_{\boldsymbol{a}' \in \mathbb{A}} e^{-E_{\boldsymbol{\theta}}(\boldsymbol{s}, \boldsymbol{a}')}}, \forall \boldsymbol{a} \in \mathbb{A} \quad (13)$$
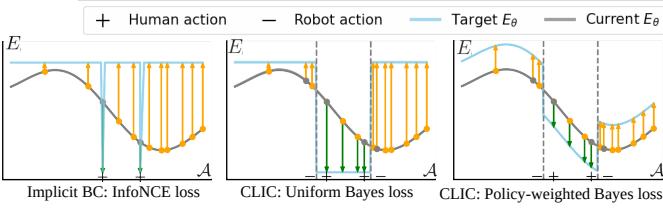
Using a uniform prior leads to a target distribution that treats sampled actions within the desired action space, $\boldsymbol{a} \in \mathbb{A} \cap \hat{\mathcal{A}}(\boldsymbol{a}^r, \boldsymbol{a}^h)$, almost equally. However, this target distribution is inaccurate as some of these actions are suboptimal. Consequently, the uniform Bayes loss can become overly optimistic by updating the policy to generate these suboptimal actions, potentially steering the policy in the wrong direction. In the following section, we introduce a conservative update loss to address this issue.

2) Policy-weighted Bayes loss: The above uniform Bayes loss treats action samples within $\mathbb{A} \cap \hat{\mathcal{A}}(\boldsymbol{a}^r, \boldsymbol{a}^h)$ almost equally and may over-optimistically lead the policy toward incorrect updates. To address this, we propose a conservative update approach when increasing $\pi_{\boldsymbol{\theta}}(\boldsymbol{a} \in \hat{\mathcal{A}}(\boldsymbol{a}^r, \boldsymbol{a}^h)|\boldsymbol{s})$. This can be achieved by defining a policy-dependent target distribution π^{target} that remains close to the current policy, assuming $p(\boldsymbol{a}|\boldsymbol{s}) = \pi_{\boldsymbol{\theta}}(\boldsymbol{a}|\boldsymbol{s})$:

$$\pi^{\text{target}}(\boldsymbol{a}|\boldsymbol{s}) \propto p(\boldsymbol{a}^h \succeq \boldsymbol{a}^r|\boldsymbol{a}, \boldsymbol{s})\pi_{\boldsymbol{\theta}}(\boldsymbol{a}|\boldsymbol{s}). \quad (14)$$

The policy $\pi_{\boldsymbol{\theta}}(\boldsymbol{a}|\boldsymbol{s})$ acts as a filter for the observation model $p(\boldsymbol{a}^h \succeq \boldsymbol{a}^r|\boldsymbol{a}, \boldsymbol{s})$. For action samples within $\hat{\mathcal{A}}(\boldsymbol{a}^r, \boldsymbol{a}^h)$, the target policy distribution π^{target} tends to assign higher probabilities to actions favored by the current policy $\pi_{\boldsymbol{\theta}}$, and lower probabilities to actions that $\pi_{\boldsymbol{\theta}}$ considers unlikely. Similarly to Eq. (13), this target distribution can be estimated using the sampled actions in $\mathbb{A}$:

$$\pi^{\text{target}}(\boldsymbol{a}|\boldsymbol{s}) = \frac{e^{-E_{\boldsymbol{\theta}}(\boldsymbol{s}, \boldsymbol{a}) + \ln p(\boldsymbol{a}^h \succeq \boldsymbol{a}^r|\boldsymbol{a}, \boldsymbol{s})}}{\sum_{\boldsymbol{a}' \in \mathbb{A}} e^{-E_{\boldsymbol{\theta}}(\boldsymbol{s}, \boldsymbol{a}') + \ln p(\boldsymbol{a}^h \succeq \boldsymbol{a}^r|\boldsymbol{a}', \boldsymbol{s})}}, \forall \boldsymbol{a} \in \mathbb{A}. (15)$$

Fig. 6: Illustration of various loss functions for training an EBM in a 1D action space. Orange dots denote action samples, with orange arrows indicating increased energy values and green arrows showing decreased energy values.

Then the loss can be calculated as in Eq. (12).

Connections to InfoNCE loss The KL loss has close connections to the InfoNCE loss used in IBC, defined in Eq. (2). By neglecting the constant term c irrelevant to the parameter $\boldsymbol{\theta}$, our KL loss can be reorganized as a weighted sum of the InfoNCE loss(See Appendix VIII-C):

$$\ell_{KL}(\boldsymbol{\theta}) \simeq \mathbb{E}_{(\boldsymbol{a}^h,\boldsymbol{a}^r,\boldsymbol{s}) \sim p_{\mathcal{D}}} \sum_{\boldsymbol{a} \in \mathbb{A}} -p(\boldsymbol{a}|\boldsymbol{a}^h \succeq \boldsymbol{a}^r, \boldsymbol{s}) \ell_{\text{InfoNCE}}(\boldsymbol{s},\boldsymbol{a},\mathbb{A}\backslash\{\boldsymbol{a}\}) + c$$

For each selected positive action $\boldsymbol{a} \in \mathbb{A}$, the InfoNCE loss decreases its energy value while increasing the value of the other sampled actions $\boldsymbol{a}' \in \mathbb{A}\backslash\{\boldsymbol{a}\}$. The key difference between InfoNCE loss and our KL loss lies in how these action samples within $\mathbb{A}$ are classified. InfoNCE loss treats all the sampled actions as negative, and only human actions as positive based on the optimal action assumption. In contrast, our KL loss classifies each action sample based on the desired action space. Specifically, the posterior probability $p(\boldsymbol{a}|\boldsymbol{a}^h \succeq \boldsymbol{a}^r, \boldsymbol{s})$ acts as a weight that quantifies how likely the selected action $\boldsymbol{a}$ is to be optimal according to the observed action pair. To combine the effects of each InfoNCE loss, the weighted average is computed for each selected action $\boldsymbol{a} \in \mathbb{A}$. As a result, actions with higher posterior probability have their energy reduced, while actions with lower posterior probability (such as $\boldsymbol{a}^r$) see their energy increased. This weighting strategy avoids overfitting by preventing the loss from being dominated by a single action label.

Here, we summarize the effects of the different loss functions. The InfoNCE loss reduces the energy of human actions while increasing the energy of all sampled actions. In contrast, our KL loss (both uniform and policy-weighted Bayes) lowers the energy of sampled actions that lie within the desired action space and raises the energy of other sampled actions. Since the action samples within the desired action space may still be suboptimal, the uniform Bayes loss can mislead the policy in the wrong update direction and may make the training process unstable. In contrast, the policy-weighted Bayes loss generates a target energy label that is closer to the existing EBM. This conservative update can mitigate the negative effects of suboptimal action samples within the desired action space, leading to a more stable training process. The differences between these loss functions are illustrated in Fig. 6.

D. Explicit Policy Shaping

While the implicit policy model can encode multi-modal feedback data, it requires longer training and inference times than explicit policies [1, 6]. Therefore, we introduce a simpli-

Fig. 7: Tasks for the simulation experiments. Each task is tested with various feedback types, including accurate demonstrations, noisy demonstrations, and relative corrective feedback. For the TwoArm-Lift task, partial feedback is also tested by applying feedback only to one of the robots.

fied version of CLIC that trains an explicit policy using the desired action space. In this subsection, we assume that the policy follows a Gaussian distribution with fixed covariance, $\pi_{\boldsymbol{\theta}}(\boldsymbol{a}|\boldsymbol{s}) \sim \mathcal{N}(\mu_{\boldsymbol{\theta}}(\boldsymbol{s}), \boldsymbol{\Sigma})$, which is a common assumption for explicit models. Under this assumption, the task is considered uni-modal, meaning there is only one optimal action for each state. Therefore, to update the policy using the observed action pair data $(\boldsymbol{a}^r, \boldsymbol{a}^h)$ at state $\boldsymbol{s}$, instead of increasing the probability of selecting actions within $\hat{\mathcal{A}}(\boldsymbol{a}^r, \boldsymbol{a}^h)$ through $\pi_{\boldsymbol{\theta}}$, we can directly enforce this probability exceeds 0.5. Formally, the objective described in Section V (increasing $\pi_{\boldsymbol{\theta}}(\boldsymbol{a} \in \hat{\mathcal{A}}(\boldsymbol{a}^r, \boldsymbol{a}^h)|\boldsymbol{s})$) is adjusted to satisfy the inequality

$$\pi_{\boldsymbol{\theta}}(\boldsymbol{a} \in \hat{\mathcal{A}}(\boldsymbol{a}^r, \boldsymbol{a}^h)|\boldsymbol{s}) \geq \pi_{\boldsymbol{\theta}}(\boldsymbol{a} \notin \hat{\mathcal{A}}(\boldsymbol{a}^r, \boldsymbol{a}^h)|\boldsymbol{s}). \quad (16)$$

Explicit policies have been extensively used for absolute corrections in unimodal tasks [51, 55, 4]. However, their application to relative corrections has been less explored. Therefore, we focus on relative corrections for this simplified version of CLIC. Notably, with the Gaussian policy assumption and a small covariance, the above inequality can be satisfied by enforcing this simplified inequality (See Appendix VIII-B):

$$\pi_{\boldsymbol{\theta}}(\boldsymbol{a}_i^-|\boldsymbol{s}) \leq \pi_{\boldsymbol{\theta}}(\boldsymbol{a}_i^+|\boldsymbol{s}), i = 1,\ldots,N_I, \quad (17)$$

where $(\boldsymbol{a}_i^-, \boldsymbol{a}_i^+)$ are the contrastive action pairs obtained from $(\boldsymbol{a}^r, \boldsymbol{a}^h)$, and are defined in Section IV. To make $\pi_{\boldsymbol{\theta}}$ satisfy the above inequality, the hinge loss can be utilized:

$$\ell(\boldsymbol{\theta}) = \mathbb{E}_{(\boldsymbol{a}^h,\boldsymbol{a}^r,\boldsymbol{s}) \sim p_{\mathcal{D}}} \sum_{i=1}^{N_I} \max(0, \log \pi_{\boldsymbol{\theta}}(\boldsymbol{a}_i^-|\boldsymbol{s}) - \log \pi_{\boldsymbol{\theta}}(\boldsymbol{a}_i^+|\boldsymbol{s})),$$

In the case of a Gaussian, this loss function simplifies to

$$\ell(\boldsymbol{\theta}; \boldsymbol{s}, \boldsymbol{a}^-, \boldsymbol{a}^+) = \max(0, ||\boldsymbol{a}^+ - \mu_{\boldsymbol{\theta}}(\boldsymbol{s})||^2 - ||\boldsymbol{a}^- - \mu_{\boldsymbol{\theta}}(\boldsymbol{s})||^2).$$

If Eq. (17) is satisfied, the mean of the Gaussian falls within the desired action space defined by the relative correction, making the loss zero. Otherwise, the loss can be used to update the parameters $\boldsymbol{\theta}$. We refer to this approach as *CLIC-Explicit*.

VI. EXPERIMENTS

In the experiment section, we demonstrate the effectiveness of our CLIC method through a series of simulations and real-world experiments. In Section VI-A, we compare CLIC with state-of-the-art methods under various types of feedback in the robot action space. Section VI-B presents an ablation study, analyzing the impact of key parameters and design choices. In Section VI-C, a 2D toy experiment highlights how CLIC prevents overfitting. Finally, Section VI-D showcases the performance of CLIC in real-robot experiments.

TABLE I: Experimental results in simulation under accurate feedback data. SR indicates the success rate, and CT represents the convergence timestep ($\times 10^3$). A '$\diagdown$' symbol denotes that the algorithm did not converge.

Method	CLIC-Half (ours)		CLIC-Circular (ours)		Diffusion Policy		Implicit BC		PVP		CLIC-Explicit (ours)		HG-DAgger	
	SR	CT	SR	CT	SR	CT	SR	CT	SR	CT	SR	CT	SR	CT
Push-T	0.931	25.6	**0.955**	28.3	0.915	24.1	0.890	31.8	0.440	28.5	0.765	35.6	0.710	38.6
Square	0.930	43.0	**0.960**	55.5	0.953	48.4	0.732	54.6	0.000	$\diagdown$	0.634	65.9	0.420	67.0
Pick-Can	0.983	37.8	**0.990**	38.4	0.980	36.1	0.688	44.2	0.000	$\diagdown$	0.995	42.5	0.990	35.7
TwoArm-Lift	0.970	18.5	**0.990**	12.6	**0.990**	23.0	0.000	$\diagdown$	0.000	$\diagdown$	0.932	14.7	0.982	14.9
Average	0.954	31.2	**0.974**	33.7	0.960	32.9	0.578	$\diagdown$	0.066	$\diagdown$	0.836	39.7	0.776	39.1

A. Simulation Experiments

Baselines We compare CLIC with multiple baselines. For explicit policies, we consider HG-DAgger [55] and D-COACH [13], which are IIL algorithms that learn from demonstration data and relative correction data, respectively. These two methods are refined for better performance, as reported in Appendix VIII-D. For implicit policies, the baselines include IBC [1], PVP [42], and Diffusion Policy [6]. As IBC and Diffusion Policy are originally offline IL methods, to make fair comparisons, we adapt them to the IIL framework to ensure fair comparisons. Within this IIL framework, all methods share the same structure, differing only in their specific policy update methods. PVP [42] employs a loss function to assign low energy values to human actions a^h and high energy values to robot actions a^r, given an observed action pair (a^r, a^h) at state s. IBC, detailed in Section III, and PVP are closely related to our method because they both involve training energy-based models. The Diffusion Policy is a counterpart method to IBC when learning from demonstrations. It outperforms IBC because of the improved training stability offered by the diffusion model. To ensure fair comparisons, we use a consistent velocity control scheme across all methods. Specifically, each method outputs a velocity command for the robot's end-effector and, if applicable, the gripper as the action at each time step.

Tasks and metrics We compared these methods across four simulated tasks, including a Push-T task introduced in [6] and three manipulation tasks from the robosuite benchmark [56], as illustrated in Fig. 7 and described in Appendix VIII-E1. The agent is trained by each method using an IIL framework, where the agent interacts with the environment and receives feedback from a **simulated teacher**. This simulated teacher is employed to guarantee repeatability and fairness in training, because human teachers may not provide consistent feedback across different experimental trials. This is an expert policy that compares its actions with those of the learner every n time steps. If the distance between these actions exceeds a threshold (set at 0.2 for all tasks), the simulated teacher provides feedback to the learner. For all the simulation tasks, we set $n = 2$. Each method was run for 160 episodes in every experiment, with this entire procedure repeated 3 times to calculate average final success rates and convergence time steps. Specifically, for each individual experiment, we calculated the final success rate by averaging the success rates of the last 8 episodes, each determined by evaluating the learned policy 10 times at the end of that episode. We defined the convergence time step as the earliest time step when the success rate exceeded 90% of the final success rate.

TABLE II: Various feedback in the action space

Type of Feedback Data	Definition
Accurate absolute correction	$a^h = a^*$
Gaussian noise	$a^h = a^* + \omega, \omega \sim \mathcal{N}(0, \|a^* - a^r\|)$
Partial feedback	$a^h \in \{[a_{r1}^*, a_{r2}], [a_{r1}, a_{r2}^*]\}$
Accurate relative correction	$a^h = a^r + eh^*, h^* = \frac{a^* - a^r}{\|a^* - a^r\|}$
Direction noise	$a^h = a^r + eh_r, \angle(h_r, h^*) = \beta \in [0, 90°)$

Feedback types In addition to accurate absolute and relative corrections, Table II summarizes other common types of feedback humans provide. These feedback types are also utilized in the simulation experiments. Here, the optimal action a^* is the original action taken by the simulated teacher. The partial feedback is utilized in the TwoArm-Lift task, where $a_{ri}, i \in \{1, 2\}$ denotes each robot's action, and a_{ri}^* denotes its optimal action.

1) Experiments with accurate feedback: Table I shows the results when the teacher's feedback has no noise.

CLIC-Half outperforms IBC, PVP, and performs on par with Diffusion Policy The results shown in Table I indicate that CLIC-Half constantly outperforms IBC and PVP in terms of success rate and convergence timesteps. PVP fails at the robosuite tasks because its loss function only considers the energy value of observed action pairs and cannot effectively shape the EBM. The optimal action assumption of IBC and Diffusion Policy is valid when the teacher's demonstration feedback is noise-free. Under such ideal conditions, this assumption should provide more informative guidance than the assumption used by CLIC-Half. However, IBC performance decreases as the action dimension of the task increases, with zero success rate in the TwoArm-Lift task. Notably, CLIC-Half achieves a 37.6% higher average success rate compared to IBC. Besides, CLIC-Half achieves a similar performance to that of Diffusion Policy. These results highlight the effectiveness of training EBMs using half-space desired action spaces.

CLIC-Circular outperforms all the baselines CLIC-Circular is the version of CLIC that mostly closely resembles IBC, as it utilizes a circular desired action space under the assumption of demonstration data. It reduces to IBC if all the three following conditions are met: (1) a very small radius defines the circular desired action space, (2) the temperature of the sigmoid function goes to zero, and (3) the uniform Bayes loss is used instead of policy-weighted Bayes loss. However, CLIC-Circular outperforms IBC by a large margin. Notably, CLIC-Circular can achieve a 99% success rate in the TwoArm-Lift task while IBC achieves zero. CLIC-Circular also outperforms CLIC-Half as it has a more strict assumption. Moreover, the fact that CLIC-Circular outperforms Diffusion Policy underscores the capacity of policies represented by

TABLE III: Simulation results under noisy demonstration data. SR: success rate, CT: convergence timestep ($\times 10^3$).

Method	CLIC-Half		CLIC-Circular		Diffusion Policy		Implicit BC		PVP		CLIC-Explicit		HG-DAgger	
	SR	CT	SR	CT	SR	CT	SR	CT	SR	CT	SR	CT	SR	CT
Gaussian noise														
Push-T	0.880	35.6	**0.960**	29.2	0.893	49.0	0.735	42.1	0.155	45.8	0.663	41.4	0.598	41.0
Square	**0.925**	64.5	0.855	63.9	0.000	＼	0.000	＼	0.000	＼	0.238	71.0	0.060	77.2
Pick-Can	0.973	37.8	**1.000**	42.8	0.467	68.2	0.070	70.4	0.000	＼	0.800	69.5	0.028	23.1
TwoArm-Lift	0.847	47.0	**0.945**	19.2	0.000	＼	0.000	＼	0.000	＼	0.433	39.3	0.008	63.8
Average	0.906	46.2	**0.933**	42.0	0.340	＼	0.268	＼	0.039	＼	0.566	53.3	0.172	35.7
Direction noise														
Push-T	0.700	48.1	**0.950**	27.3	0.187	67.9	0.574	55.5	0.000	＼	0.638	44.6	0.473	43.6
Square	0.870	63.6	**0.910**	58.9	0.125	75.8	0.230	70.4	0.000	＼	0.161	66.9	0.128	71.6
Pick-Can	**1.000**	43.1	**1.000**	39.0	0.000	＼	0.482	81.4	0.000	＼	0.867	55.4	0.342	72.0
TwoArm-Lift	0.965	18.7	**0.980**	16.5	0.885	46.6	0.000	＼	0.000	＼	0.807	21.0	0.157	31.4
Average	0.884	43.4	**0.960**	35.4	0.399	＼	0.429	＼	0.000	＼	0.618	47.0	0.275	54.7

EBMs to surpass their diffusion-based counterparts. Therefore, while previous studies [7, 6] highlight the challenges of training EBMs, our results indicate that EBM-based policies can be trained reliably using demonstration data, by leveraging the concept of the desired action space.

CLIC-Explicit achieves good results in uni-modal tasks, whereas PVP performs poorly The losses used by PVP and CLIC-Explicit share a critical similarity: they both increase the probability of human actions and decrease that of robot actions. We denote this loss type as *point-based loss* as it calculates the loss only on observed action pairs. In contrast, the losses for CLIC-Half, CLIC-Circular, and IBC are termed *set-based loss*. These losses utilize not only observed action pairs but also additional actions sampled from the EBM for loss calculation. Notably, PVP has zero success rate at robosuite tasks, whereas CLIC-Explicit performs well in Pick-Can and TwoArm-Lift—tasks that are both unimodal and align with the Gaussian policy assumption. Since PVP employs an EBM as its policy and CLIC-Explicit uses a Gaussian-parametrized policy, the result suggests that point-based loss is only effective for policies with simple forms, such as those based on Gaussian distributions, and fails to shape complex policies like EBMs. In contrast, the set-based loss provides richer information and is more effective for training EBMs.

2) Experiments with noisy demonstration feedback: Noise is common when human teachers provide feedback to robots, either for absolute or relative corrections. This can arise due to factors such as human fatigue or the limitations of teleoperation devices. Therefore, it is essential for algorithms to account for such noise. To evaluate the ability of CLIC and baseline methods to learn from noisy feedback, we implemented two types of noise in simulation, as defined in Table II. For absolute corrections, we use a Gaussian distribution to model the noise, which is added to the original demonstration data. For relative corrections, the feedback is derived from absolute correction with a known magnitude. To introduce noise, we perturb the original direction signal by $45°$ while maintaining its magnitude.

CLIC remains robust while baselines degrade under noisy feedback The results in Table III show that, as feedback transitions from accurate to noisy, CLIC-Half and CLIC-Circular experience much smaller performance drops compared to the other baselines. This can be observed by comparing Table II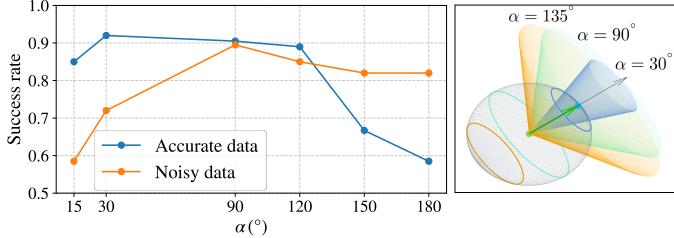I with Table I. In contrast, methods like Diffusion Policy and IBC perform significantly worse under noisy conditions. This difference arises because these baselines depend on the strict assumption of having accurate demonstrations, making them unable to handle noisy feedback effectively. In comparison, CLIC allows adjusting the desired action space through hyperparameters, ensuring that the true optimal action remains within the desired action space even under noisy feedback. This capability helps maintain robust performance under noisy conditions.

3) Experiments with relative or partial feedback: When providing demonstrations is not possible, humans can provide feedback in more flexible ways, offering valuable information to guide improvement. One such scenario involves partial feedback, where limitations in the control interface or a large action space make it challenging to provide complete demonstrations. In this case, we evaluated all methods on the TwoArm-Lift task, in which the teacher provides demonstration feedback to only one robot at a time. Another scenario involves relative corrective feedback. This feedback type is easier to provide than demonstration, because it does not require the teacher to know precisely which action should be taken; instead, it only necessitates an understanding of the general behavior the robot should exhibit. To assess how effectively the methods handle this feedback type, we conducted experiments across four simulation tasks.

CLIC-Half and CLIC-Explicit effectively learn from partial feedback The results of partial feedback experiments are shown in Table IV. In these experiments, human actions consist of two parts: actions on the *feedback dimensions* (where human feedback is provided) and actions on the *non-feedback dimensions* (which may be suboptimal). While CLIC-Half maintains its success rate when transitioning from accurate demonstration to partial feedback, Diffusion Policy suffers from lower success rates and longer convergence times. This difference arises because the BC loss in Diffusion Policy attempts to imitate the entire teacher action, including non-feedback dimensions, potentially leading to suboptimal behaviors. In contrast, CLIC-Half imitates a desired action space rather than a single action label. It focuses on improving actions on the feedback dimensions while leaving the non-feedback dimensions unconstrained. As a result, CLIC-Half is robust to partial feedback as long as the optimal action lies within the desired action space. The same reasoning explains the results of CLIC-Explicit outperforming HG-DAgger. On

TABLE IV: Simulation results under partial and relative feedback data. SR: success rate, CT: convergence timestep ($\times 10^3$).

Method	CLIC-Half		CLIC-Circular		Diffusion Policy		Implicit BC		PVP		CLIC-Explicit		D-COACH	
	SR	CT	SR	CT	SR	CT	SR	CT	SR	CT	SR	CT	SR	CT
Partial feedback														
TwoArm-Lift	**0.990**	26.9	0.920	17.8	0.897	29.7	0.000	\	0.000	\	0.863	18.1	0.687	25.7
Relative correction														
Push-T	**0.853**	40.8	0.000	\	0.060	72.0	0.400	58.8	0.110	50.4	0.733	43.5	0.520	49.0
Square	**0.940**	65.6	0.000	\	0.000	\	0.005	56.3	0.000	\	0.065	66.1	0.243	79.7
Pick-Can	**0.983**	41.9	0.000	\	0.000	\	0.310	81.7	0.000	\	0.890	67.2	0.693	62.8
TwoArm-Lift	**0.955**	25.3	0.000	\	0.000	\	0.000	\	0.000	\	0.920	16.8	0.115	64.7
Average	**0.933**	**43.4**	0.000	\	0.015	\	0.346	\	0.066	\	0.652	48.4	0.393	64.1

Fig. 8: Hyperparameter analysis of the directional certainty parameter α for CLIC-Half. The right figure visualizes how different values of α adjust the desired action space in 3D.
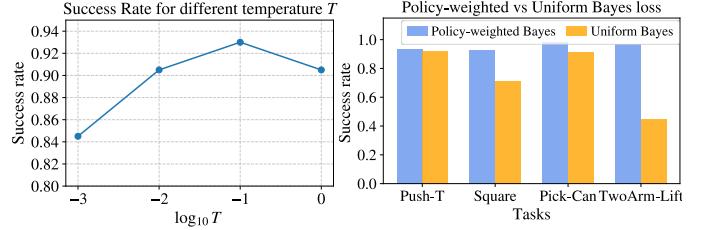

Fig. 9: Ablation study: (1) effects of the temperature parameter T. (2) Policy-weighted Bayes loss vs uniform Bayes loss.

the other hand, CLIC-Circular's performance drops because its circular desired action space might not include the optimal action. This result highlights the importance of ensuring the assumption of CLIC aligns with the data.

CLIC-Half and CLIC-Explicit can learn from relative corrective feedback The results of relative corrective feedback are reported in Table IV. In these experiments, human actions improve upon robot actions but are not optimal. CLIC-Half and CLIC-Explicit show only small performance drops compared to results in absolute corrections in Table I, because the correction magnitude information is unknown in relative correction. In contrast, all demonstration-based baselines fail completely, achieving near-zero success rates. This failure occurs because the BC loss can mislead policy updates, especially when the current policy's actions are better than the human actions in the dataset. Meanwhile, CLIC-Half and CLIC-Explicit construct desired action spaces to update the policy; as the policy improves, these spaces constructed from the dataset do not conflict with it and are still useful for policy improvement. Additionally, CLIC-Circular fails with a zero success rate, as its circular desired action space fails to include the optimal action. Overall, the ability of CLIC-Half and CLIC-Explicit to learn from relative corrective feedback highlights their distinct advantages in such scenarios.

B. Ablation Study

In this section, we analyze the impact of various hyperparameters and loss design choices on the performance of the CLIC method. Specifically, we focus on the directional certainty parameter α, the temperature T used in the sigmoid function of the observation model, and the different assumptions regarding the prior probability $p(\boldsymbol{a}|\boldsymbol{s})$. During these experiments, CLIC-Half is utilized.

1) Effects of directional certainty α : The angle α is the main parameter utilized to control the shape of the desired
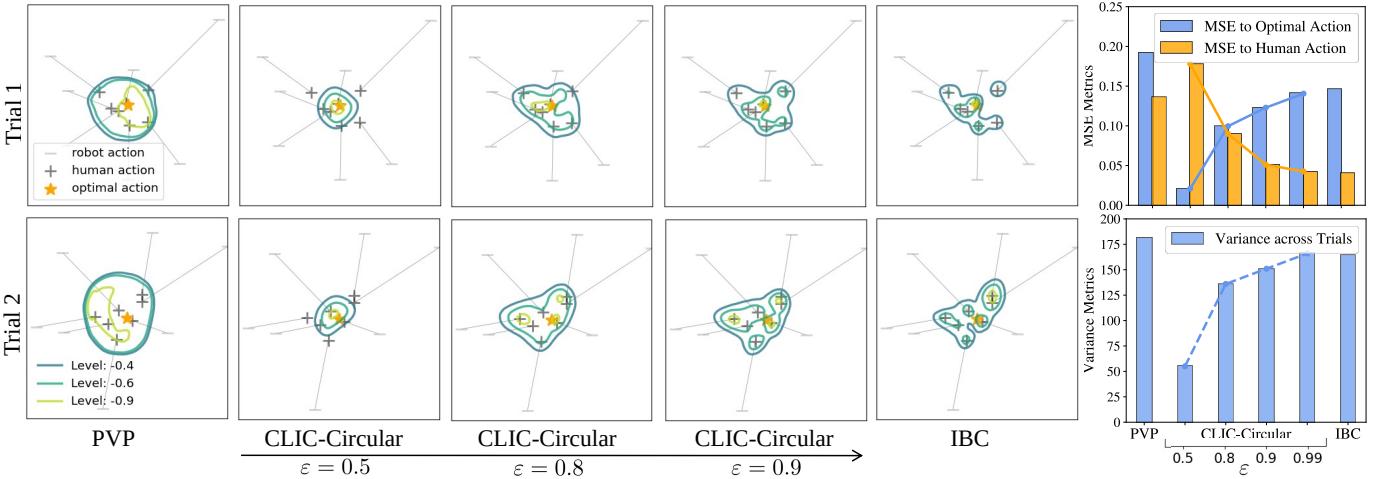
action space for CLIC-Half, as shown in the right part of Fig. 8. In this experiment, we carried out experiments in the Square task. Two feedback types were considered, one with accurate feedback and another with direction noise (noise angle $\beta = 45°$). The results are reported in the left part of Fig. 8. For accurate feedback cases, the success rate decreases when α is larger than $120°$. This occurs because increasing α expands the desired action space to include more undesired actions, thereby providing less useful information for updating the EBM. For direction noise, the success rate decreases for $\alpha < 2\beta = 90°$. This is because for any given feedback with $\alpha < 2\beta$, the desired action space fails to include the optimal action and misguides the EBM in its update process. These findings highlight the importance of carefully selecting α to balance the trade-off: maintaining an informative desired action space and ensuring that it includes the optimal action.

2) Effects of temperature T: In Section V-B, the temperature T is utilized to control the sharpness of the probability distribution $\Pr[\boldsymbol{a} \in \mathcal{A}(\boldsymbol{a}^r, \boldsymbol{a}^h)|\boldsymbol{a}, \boldsymbol{s}]$. We study the effects of T in this experiment on the performance of CLIC, where four different values of T are tested in the Square task. The results are presented in the left side of Fig. 9. When T is very small ($\log_{10} T = -3$), the success rate drops sharply. At this extreme, the observation model becomes binary (0/1), creating a sharp boundary that is difficult for the neural network to learn. Conversely, when T is too large ($T = 1$), the success rate also declines. In this case, the probabilities of actions belonging or not belonging to $\mathcal{A}(\boldsymbol{a}^r, \boldsymbol{a}^h)$ become nearly indistinguishable, offering limited information for policy improvement. $T = 0.1$ proves to be a good balance between these extremes and is selected across all experiments for CLIC-Half.

3) Policy-weighted Bayes loss vs Uniform Bayes loss: As described in Section V-C1, the uniform Bayes loss treats all actions within the desired action space equally, whereas the policy-weighted Bayes loss prioritizes actions closer to the current robot's policy. To evaluate the effectiveness of the policy-weighted Bayes loss, we compared it against the

Fig. 10: Learned EBM landscapes across different trials. The figure compares the energy landscapes learned by CLIC, PVP, and IBC after training in a 2D action space. Each row corresponds to the resulting EBMs of each trial. In the middle part, we visualize the process of how CLIC-Circular reduces to IBC as ε increases. CLIC-Circular (with $\varepsilon = 0.5$) effectively trains EBM across different trials, leading to consistent minima close to the true optimal action. In contrast, IBC overfits human actions and fails to estimate the true optimal action. Three evaluation metrics are shown in the right part of the figure.

uniform Bayes loss. We implement the uniform variant of CLIC and evaluate it across four simulation tasks with accurate demonstration feedback. The results, shown in the right side of Fig. 9, demonstrate that the uniform Bayes loss leads to significantly poorer performance compared to the policy-weighted Bayes loss. This highlights the importance of incremental policy updates. Since the desired action space may include some undesired actions, staying close to the current policy helps avoid imitating unintended behaviors, resulting in a more stable training process.

C. Toy Experiments on Noisy Feedback

In this section, we present an example to illustrate the improved performance of CLIC over IBC. The toy task in this example consists of a single constant state with a 2D action space, where the optimal action is set to $\mathbf{0}$ (see Fig. 10). The objective is to estimate the optimal action through multiple corrective feedback. We carried out experiments over 10 trials. In each trial, we generated a randomly sampled dataset consisting of 6 or 7 data points $(\boldsymbol{s}, \boldsymbol{a}^r, \boldsymbol{a}^h)$, where human actions were drawn from a Gaussian distribution centered at the optimal action. Each method was trained for 1,000 steps in an offline IL setting, and we visualized the trained EBMs for each method for the first two trials in Fig. 10.
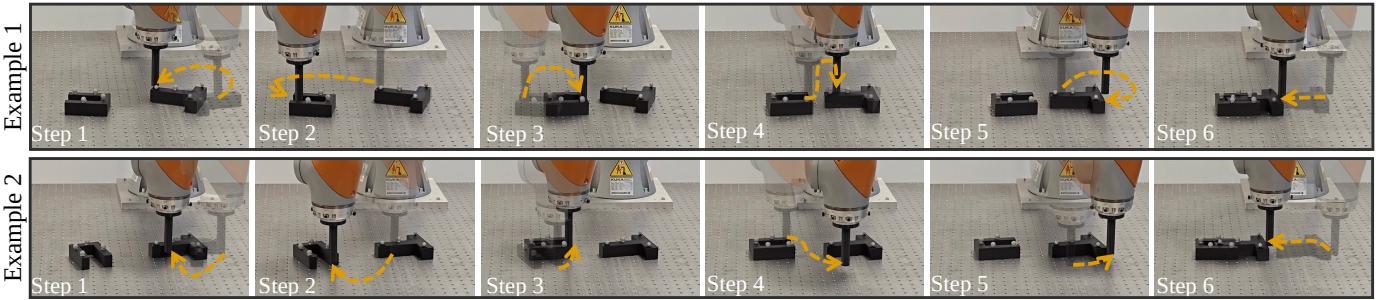
To evaluate the methods, we introduced three metrics: (1) the mean square error (MSE) to optimal action: this measures MSE between each local minimum action of the EBM and the optimal action. (2) MSE to human action: this calculates the average MSE between each local minimum action of the EBM and its nearest human action. A smaller value indicates that the EBM is overfitting to the human action. (3) Variance across trials: this evaluates the variance of the EBM values over the entire action space across ten different trials. These metrics are computed by averaging the results over the 10 trials and are reported in the right side of Fig. 10.

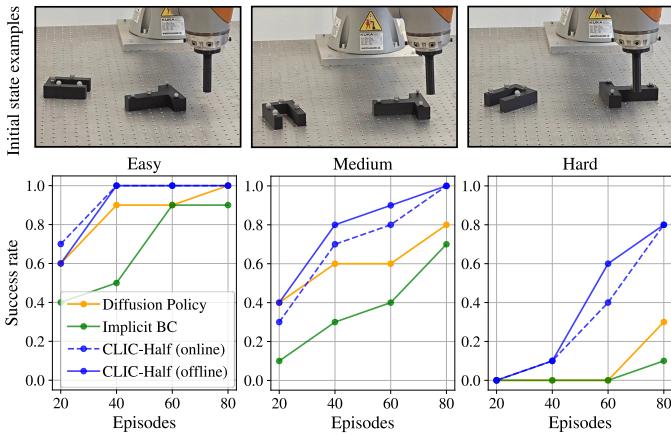**CLIC learns consistent EBM landscapes across different trials** The PVP-trained EBM tends to be over-optimistic about favorable actions by outputting low energy values for a large region of actions that are not present in the dataset, as shown in the left side of Fig. 10. This occurs because PVP calculates its loss using only observed action pairs, leaving the energy values of other actions in the action space uncontrolled. On the other hand, IBC's loss function encourages human actions and discourages all other actions, even actions that are very similar to human actions. Consequently, the IBC-trained EBM overfits the data, learning minima corresponding to individual human actions. This overfitting results in EBM landscapes with high variance across different trials, as shown in the bottom-right figure of Fig. 10. In contrast, the CLIC-trained EBM maintains consistent landscapes, with minima close to the true optimal action and low variance across different trials. This explains the superior performance of CLIC over IBC and PVP, as observed in Section VI-A1.

CLIC-Circular reduces to IBC under stricter assumptions To illustrate how CLIC-Circular reduces to IBC, we progressively decrease the radius of the circular desired action spaces by increasing the value of ε (see the middle part of Fig. 10). As ε increases, the CLIC-trained EBM starts to split into several clusters and overfit data labels with smaller MSE to human actions, as reported in the right part of Fig. 10. This overfitting also leads to a larger MSE to the optimal action, indicating that the EBM becomes less effective at identifying the optimal action. Eventually, as $\varepsilon \to 1$, the EBM landscape closely resembles the one trained using IBC. When the radius becomes nearly zero, imitating a circular desired action space reduces to imitating a human action label, leading to overfitting and performance drops. This observation highlights the key distinction between CLIC-Circular and IBC: imitating a circular desired action space rather than a single action. This distinction is crucial for training EBMs stably.

Fig. 11: Examples of CLIC-Half policy rollout for the Insert-T task after training. At each step, the transparent figure shows the initial state, and the orange arrow indicates the end-effector's trajectory. The solid figure illustrates the resulting end state, which becomes the initial state for the next step.

Fig. 12: Experiment results for the Insert-T task, categorized by difficulty levels (easy, medium, and hard). Each column shows the performance metrics for a given difficulty level, along with examples of initial states for that level. "CLIC-Half (offline)" denotes results for CLIC-Half trained offline.
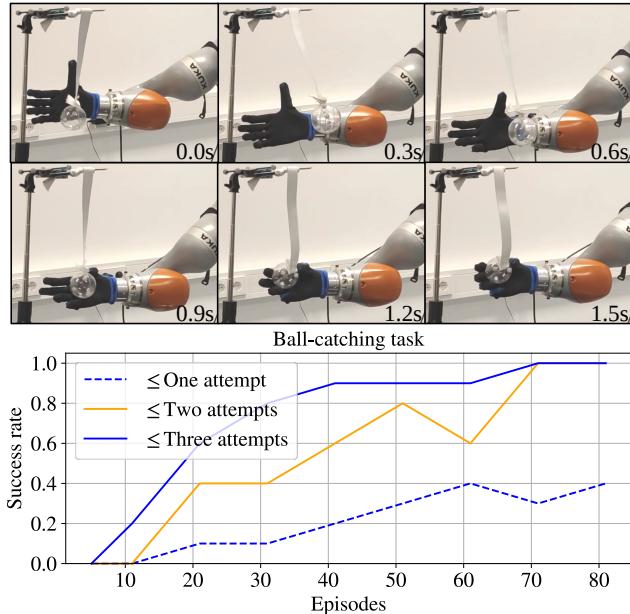
D. Real-robot Validations

Here, we use three tasks to demonstrate the practical applicability of CLIC. The experiments include a long-horizon multi-modal Insert-T task, a dynamic ball-catching task, and a water-pouring task that necessitates precise control of the robot's end effector position and orientation. For the Insert-T task, we employ CLIC-Half and compare its performance against IBC and Diffusion Policy. For the ball-catching and water-pouring tasks, we use CLIC-Explicit because it performs well in uni-modal tasks, as demonstrated in Section VI-A, and is more time-efficient compared to CLIC with an EBM policy (Details in Appendix VIII-F.). The experiments were carried out using a 7-DoF KUKA iiwa manipulator. When required, an underactuated robotic hand (1-dimensional action space) was attached to its end effector. A 6D space mouse was employed to provide feedback on the pose of the robot's end effector. Furthermore, in the ball-catching task, a keyboard provided feedback on the gripper's actuation. The setup of each task is detailed in Appendix VIII-E2, and the time durations used are reported in Appendix VIII-E3. The experiment results are reported as follows:

1) Insert-T—a comparison between state-of-the-art methods: The Insert-T task requires the robot to insert a T-shaped object into a U-shaped object by pushing to adjust their positions and orientations. Compared to the Push-T task in simulation experiments, Insert-T is more complex due to two factors: (1) it involves two objects, introducing multi-modal decisions about which object to manipulate first; and (2) it has an increased task horizon. This makes Insert-T a valuable benchmark for evaluating CLIC's performance in long-horizon, multi-modal tasks compared to state-of-the-art methods. To better analyze the performance of each method, we categorize the task into three difficulty levels based on the initial state of the objects and the number of contact changes required to complete the task (according to the teacher's policy). Examples of these categories are shown in the upper part of Fig. 12. Tasks requiring fewer than 1 contact change are classified as "easy", fewer than 5 as "medium", and 5 or more as "hard". During each evaluation, 10 different initial states are tested for each category. To ensure a fair comparison, all methods are evaluated using the same set of initial states. In the experiment, human-provided demonstration feedback is used to train CLIC-Half within the IIL framework. The collected data is also used to train baseline methods (Diffusion and IBC) offline. For a fair comparison, CLIC is additionally trained offline on the same dataset as the baselines.

Results for different difficulty levels are shown in Fig. 12. For easy tasks, baseline methods perform similarly to CLIC but converge more slowly. For medium and hard tasks, CLIC achieves significantly higher success rates. This is particularly evident for hard tasks, where CLIC achieves 80% success compared to 30% for Diffusion and 10% for IBC. The results demonstrate CLIC's ability to handle complex multi-modal tasks, thanks to the powerful encoding capabilities of EBMs and CLIC's stable EBM training. Furthermore, as the task difficulty increases, CLIC outperforms Diffusion and IBC by a large margin. This suggests that, for training policies, using a desired action space is more robust and efficient in real-robot tasks than relying on a single action label. Examples of post-training policy rollouts for CLIC in hard tasks are shown in Fig. 11.

Note that CLIC is an interactive learning method, whereas Diffusion and IBC are offline methods in this experiment. Figure 12 also includes results for CLIC trained with offline data, showing a similar final success rate to the online version. This indicates that CLIC can be employed to learn from offline data as well. While CLIC is primarily based on the
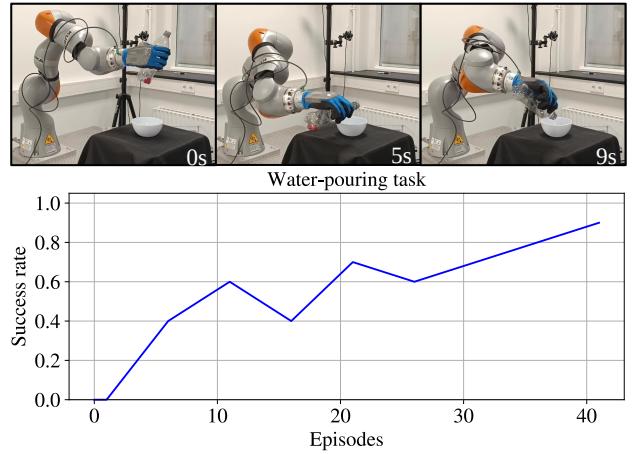
Ball-catching task

Fig. 13: Experiment results for the ball-catching task.

Water-pouring task

Fig. 14: Experiment results for the water-pouring task.

IIL framework, the core ideas proposed here could also benefit offline methods. We believe exploring offline training of CLIC is a promising direction for future work.

2) Ball catching—quick coordination and partial feedback: The ball-catching task is challenging because of its highly dynamic nature. This complexity makes it difficult to provide successful demonstrations of the task to the robot, thus ruling out demonstration-based IIL methods for solving it[1]. Instead, relative corrective feedback is more intuitive and easier for this task as humans can provide direction signals occasionally to improve the robot's policy [57]. Besides, for a successful grasp, the robot must coordinate precisely the ball's motion, the end-effector's motion, along with the gripper's actuation. This requirement makes it challenging to provide feedback on the complete action space at any given moment, and makes partial feedback suitable for this task. With partial feedback, relative corrections can be independently provided for either the end-effector's motion or the gripper's actuation. Therefore, this task enables testing CLIC's ability to learn effective policies from relative corrective feedback that is also partial.

Fig. 13 shows the experiment results of the ball-catching task, reporting the success rate of catching the ball within one, two, and three attempts. By the end of training, the robot achieves a 1.0 success rate for catching the ball within two attempts, and its first-attempt success rate continues to improve to 0.4. One post-training policy rollout of a successful first-attempt catch is shown in Fig. 13, where the ball is caught within 1.5 seconds, an impressive result given the actuation delay of the robot hand. This experiment demonstrates that CLIC can leverage both the relative corrective feedback and partial feedback effectively to learn challenging high-frequency tasks.

3) Water pouring—learning full pose control with CLIC: The water-pouring task requires the robot to control the pose of a bottle to precisely pour liquid (represented with marbles)

into a small bowl. CLIC-Explicit is utilized in this experiment. The human teacher can provide either absolute or relative corrective feedback and has the flexibility to switch between these modes by pressing a specific keyboard button. Initially, absolute feedback was preferred as the policy was learned from scratch, and it was easier to intervene in a 6D action space. As the policy improved, relative corrections made it easier to refine the policy in specific regions of the state space.

The experimental data is shown in Fig. 14. From Episode 1 to Episode 16, the teacher's feedback is provided in an absolute correction format. From Episode 16 onward, the teacher's feedback is given as relative corrections to make small adjustments to the robot's policy. The success rate exhibits an overall improving trend, consistently increasing from 0.6 in Episode 26 to 0.9 by Episode 41. An example of the policy rollouts after training is illustrated in Fig. 14. This experiment demonstrates the effectiveness of CLIC for learning precise control over position and orientation.

VII. CONCLUSION

In this paper, we introduce CLIC, a novel approach to learning policies from interactive human corrections. To achieve this, the desired action space concept and its probabilistic formulation are presented. These are employed to design a novel loss function to align the robot's policy with desired action spaces. Our extensive experiments in both simulation and real-world experiments demonstrate the advantages of CLIC over state-of-the-art methods. Notably, CLIC's loss function overcomes the overfitting problem inherent in behavior cloning. As a result, CLIC is applicable to a broader range of feedback types and efficiently achieves robust and stable performance with an EBM-based policy.

Despite the demonstrated effectiveness of CLIC in simulations and real-world experiments, there are limitations that future work can improve. Firstly, similar to HG-DAgger, our method does not utilize the robot's state-action data when the teacher provides no feedback [48]. In future work, we plan to investigate how to incorporate these non-intervention data into CLIC. Secondly, CLIC relies on learner's errors to trigger corrective feedback. This can be a limitation because if the learner initially performs well, our method may not effectively improve the robot's policy. One potential solution

---

[1]This limitation could be overcome with a highly reactive and precise teleoperation device. However, this also makes the solution more expensive.

is to incorporate evaluative feedback to reinforce learner's successful behaviors. Beyond these limitations, several promising directions for future research include offline training of CLIC and applying the CLIC loss to train diffusion or flow-based models.

VIII. APPENDIX

A. Proof for the Convergence of Overall Desired Action Space

Proposition 1: For any state s, assume a trained policy $\pi_{\boldsymbol{\theta}}$ always select actions from $\hat{\mathcal{A}}_k^{\mathcal{D}(s)}$, and there are a finite number of optimal actions. Assume that there is a nonzero probability for the teacher to provide feedback to each suboptimal action $\boldsymbol{a}_{k+1}^r \sim \pi_{\boldsymbol{\theta}}(\cdot|s)$. Then, as $k \to \infty$, $\hat{\mathcal{A}}_k^{\mathcal{D}(s)}$ converges to $\mathcal{A}^*(s)$ or a subset of $\mathcal{A}^*(s)$.

Proof: For any state s, the combined desired action space is denoted as $\mathcal{A}_k^{\mathcal{D}(s)}$. As we assume $\pi_{\boldsymbol{\theta}}(\boldsymbol{a} \in \mathcal{A}_k^{\mathcal{D}(s)}|s) = 1$, for any action a_{k+1}^r sampled from the policy $\pi_{\boldsymbol{\theta}}(\cdot|s)$, it is also inside the combined desired action space, i.e., $a_{k+1}^r \in \mathcal{A}_k^{\mathcal{D}(s)}$. If a_{k+1}^r is suboptimal, the feedback $\boldsymbol{a}_{k+1}^h$ is provided accordingly, resulting in a new desired action space $\hat{\mathcal{A}}(\boldsymbol{a}_{k+1}^r, \boldsymbol{a}_{k+1}^h)$.

If $\hat{\mathcal{A}}^{\mathcal{D}_k(s)} \cap \hat{\mathcal{A}}(\boldsymbol{a}_{k+1}^r, \boldsymbol{a}_{k+1}^h) \neq \varnothing$, then the new feedback $\boldsymbol{a}_{k+1}^h$ reduce the volume of $\mathcal{A}_{k+1}^{\mathcal{D}(s)}$ as

$$\mathcal{A}_{k+1}^{\mathcal{D}(s)} = \hat{\mathcal{A}}^{\mathcal{D}_k(s)} \cap \hat{\mathcal{A}}(\boldsymbol{a}_{k+1}^r, \boldsymbol{a}_{k+1}^h) \subset \mathcal{A}_k^{\mathcal{D}(s)} \quad (18)$$

If $\hat{\mathcal{A}}^{\mathcal{D}_k(s)} \cap \hat{\mathcal{A}}(\boldsymbol{a}_{k+1}^r, \boldsymbol{a}_{k+1}^h) = \varnothing$, the new feedback $\boldsymbol{a}_{k+1}^h$ is associate to an optimal action that is outside $\mathcal{A}_k^{\mathcal{D}(s)}$, therefore increasing the volume of $\mathcal{A}_{k+1}^{\mathcal{D}(s)}$ as

$$\mathcal{A}_k^{\mathcal{D}(s)} \subset \mathcal{A}_{k+1}^{\mathcal{D}(s)} = \hat{\mathcal{A}}^{\mathcal{D}_k(s)} \cup \hat{\mathcal{A}}(\boldsymbol{a}_{k+1}^r, \boldsymbol{a}_{k+1}^h) \quad (19)$$

However, the total number of times of doing expansion of $\mathcal{A}_k^{\mathcal{D}(s)}$ is bounded by the number of optimal actions N_*, which is finite by assumption.

Therefore, as the feedback number goes to infinite, the volume of $\mathcal{A}_k^{\mathcal{D}(s)}$ continues to decrease. Since each desired action space includes at least one optimal action, by applying intersection, the combined desired action space still contains at least one the optimal action. By expansion, the number of included optimal actions increases. In other words, this process of interactive corrections leads to a non-empty $\mathcal{A}_k^{\mathcal{D}(s)}$ that includes at least one optimal action. In the limit, all actions in $\mathcal{A}_k^{\mathcal{D}(s)}$ are optimal and will not receive any feedback. Hence,

$$\lim_{k \to \infty} \mathcal{A}_k^{\mathcal{D}(s)} \subset \mathcal{A}^*(s).$$

$\blacksquare$

B. Proof of the Simplified CLIC-Explicit Objective

We want to prove that, with the Gaussian distribution assumption, Eq. (16) can be satisfied by satisfying Eq. (17).

Proof: As the probability of sampling actions within $\hat{\mathcal{A}}(\boldsymbol{a}^r, \boldsymbol{a}^h)$ using $\pi_{\boldsymbol{\theta}}$ can be defined as

$$\pi_{\boldsymbol{\theta}}(\boldsymbol{a} \in \hat{\mathcal{A}}(\boldsymbol{a}^r, \boldsymbol{a}^h)|s) = \int_{\boldsymbol{a} \in \mathcal{A}} \pi_{\boldsymbol{\theta}}(\boldsymbol{a}|s) \Pr[\boldsymbol{a} \in \hat{\mathcal{A}}(\boldsymbol{a}^r, \boldsymbol{a}^h)|\boldsymbol{a}, s] d\boldsymbol{a}$$

$$\overset{T \to 0}{=} \int_{\boldsymbol{a} \in \mathcal{A}} \pi_{\boldsymbol{\theta}}(\boldsymbol{a}|s) \cdot \mathbf{1}_{\boldsymbol{a} \in \hat{\mathcal{A}}(\boldsymbol{a}^r, \boldsymbol{a}^h)} d\boldsymbol{a},$$

Then Eq. (16) in equivalent to

$$\int_{\boldsymbol{a} \in \mathcal{A}} \pi_{\boldsymbol{\theta}}(\boldsymbol{a}|s) \left(2 \cdot \mathbf{1}_{\boldsymbol{a} \in \hat{\mathcal{A}}(\boldsymbol{a}^r, \boldsymbol{a}^h)} - 1 \right) d\boldsymbol{a} \geq 0 \quad (20)$$

As $\pi_{\boldsymbol{\theta}}(\boldsymbol{a}|s) \sim \mathcal{N}(\boldsymbol{\mu}_{\boldsymbol{\theta}}(s), \boldsymbol{\Sigma})$, we have

$$\pi_{\boldsymbol{\theta}}(\boldsymbol{a}|s) \propto \exp\left(-\frac{1}{2}(\boldsymbol{a} - \boldsymbol{\mu}_{\boldsymbol{\theta}}(s))^\mathsf{T} \boldsymbol{\Sigma}^{-1} (\boldsymbol{a} - \boldsymbol{\mu}_{\boldsymbol{\theta}}(s)) \right), \quad (21)$$

Without loss of generality, we set $\boldsymbol{\Sigma} = \sigma \boldsymbol{I}$ proportional to the identity matrix. Then, from $\pi_{\boldsymbol{\theta}}(\boldsymbol{a}_i^-|s) < \pi_{\boldsymbol{\theta}}(\boldsymbol{a}_i^+|s)$, we have

$$\|\boldsymbol{a}_i^+ - \boldsymbol{\mu}_{\boldsymbol{\theta}}(s)\|^2 < \|\boldsymbol{a}_i^- - \boldsymbol{\mu}_{\boldsymbol{\theta}}(s)\|^2,$$

which means that $\boldsymbol{\mu}_{\boldsymbol{\theta}}(s) \in \hat{\mathcal{A}}(\boldsymbol{a}^r, \boldsymbol{a}^h)$. For $\alpha = 180°$, $\hat{\mathcal{A}}(\boldsymbol{a}^r, \boldsymbol{a}^h)$ is a half-space and $2 \cdot \mathbf{1}_{\boldsymbol{a} \in \hat{\mathcal{A}}(\boldsymbol{a}^r, \boldsymbol{a}^h)} - 1 > 0$ always holds, thus Eq. (20) always holds. For $\alpha \in (0°, 180°)$, extra assumption needs to be made regarding the variance σ to make Eq. (20) holds. For the extreme case, we can choose a $\sigma \to 0$ such that the policy outputs only the mean. In this case, Eq. (20) holds. $\blacksquare$

C. Policy-weighted Bayes Loss and InfoNCE Loss

In this section, we detail the connections between Policy-weighted Bayes Loss and InfoNCE loss:

$$\mathrm{KL}\left(p(\boldsymbol{a}|\boldsymbol{a}^h \succeq \boldsymbol{a}^r, s) \| \pi_{\boldsymbol{\theta}}(\boldsymbol{a}|s) \right)$$

$$= -\mathop{\mathbb{E}}_{\boldsymbol{a} \sim p(\boldsymbol{a}|\boldsymbol{a}^h \succeq \boldsymbol{a}^r, s)} \log \pi_{\boldsymbol{\theta}}(\boldsymbol{a}|s) + \mathop{\mathbb{E}}_{\boldsymbol{a} \sim p(\boldsymbol{a}|\boldsymbol{a}^h \succeq \boldsymbol{a}^r, s)} \log p(\boldsymbol{a}|\boldsymbol{a}^h \succeq \boldsymbol{a}^r, s)$$

$$= -\mathop{\mathbb{E}}_{\boldsymbol{a} \sim p(\boldsymbol{a}|\boldsymbol{a}^h \succeq \boldsymbol{a}^r, s)} \log \pi_{\boldsymbol{\theta}}(\boldsymbol{a}|s) + c$$

$$\simeq \sum_{\boldsymbol{a} \in \mathbb{A}} -p(\boldsymbol{a}|\boldsymbol{a}^h \succeq \boldsymbol{a}^r, s) \log \pi_{\boldsymbol{\theta}}(\boldsymbol{a}|s) + c$$

$$\overset{Eq.(13)}{\simeq} \sum_{\boldsymbol{a} \in \mathbb{A}} -p(\boldsymbol{a}|\boldsymbol{a}^h \succeq \boldsymbol{a}^r, s) \log \frac{e^{-E_{\boldsymbol{\theta}}(s, \boldsymbol{a})}}{\sum_{\boldsymbol{a}' \in \mathbb{A}} e^{-E_{\boldsymbol{\theta}}(s, \boldsymbol{a}')}} + c$$

$$\overset{Eq.(2)}{=} \sum_{\boldsymbol{a} \in \mathbb{A}} -p(\boldsymbol{a}|\boldsymbol{a}^h \succeq \boldsymbol{a}^r, s) \ell_{\text{InfoNCE}}(s, \boldsymbol{a}, \mathbb{A} \backslash \{\boldsymbol{a}\}) + c,$$

where c denotes the constant that does not depend on $\boldsymbol{\theta}$. By plugging the above equation into Eq. (12), the KL loss becomes

$$\ell_{KL}(\boldsymbol{\theta}) \simeq \mathop{\mathbb{E}}_{(\boldsymbol{a}^h, \boldsymbol{a}^r, s) \sim p_{\mathcal{D}}} \sum_{\boldsymbol{a} \in \mathbb{A}} -p(\boldsymbol{a}|\boldsymbol{a}^h \succeq \boldsymbol{a}^r, s) \ell_{\text{InfoNCE}}(s, \boldsymbol{a}, \mathbb{A} \backslash \{\boldsymbol{a}\}) + c$$

D. Details of the Implementation of Baselines

1) D-COACH: In D-COACH, the teacher shapes policies $\pi(\boldsymbol{a}|s) \sim \mathcal{N}(\boldsymbol{\mu}_{\boldsymbol{\theta}}(s), \boldsymbol{\Sigma})$ by giving occasional relative corrective feedback $\boldsymbol{h}$. The human action $\boldsymbol{a}^h = \boldsymbol{a}^r + e\boldsymbol{h}$ is employed to update the policy parameters $\boldsymbol{\theta}$ in a behavior cloning manner:

$$\ell_\pi^{\text{COACH}}(s) = \min_{\boldsymbol{\theta}} \|\boldsymbol{\mu}_{\boldsymbol{\theta}}(s) - \boldsymbol{a}^h\|^2. \quad (22)$$

However, when learning from past experiences by using a replay buffer, as $\boldsymbol{a}^h \neq \boldsymbol{a}^*$, old feedback can lead the policy in the wrong direction. Consequently, to avoid this, D-COACH keeps a small data buffer $\mathcal{D}$, using only recent feedback for policy updates. This approach leads to overfitting to recent trajectories and reduced learning efficiency.

To address this issue, batched D-COACH [40], BD-COACH for short, was proposed, which is used as the baseline in Section VI-A3. Here, besides learning a policy, BD-COACH learns a human model $H_\phi(\boldsymbol{a}, s) = \boldsymbol{h}$. This model estimates the human's relative corrective feedback $\boldsymbol{h}$ given the robot's

TABLE V: Tasks summary

Tasks	State dim	Action dim	Multi-modal	Contact Rich	High freq
Push-T	24	2	✓	✓	✗
Square	48	7	✓	✗	✗
Pick-Can	40	7	✗	✗	✗
TwoArm-Lift	48	14	✗	✗	✗
Ball-catching	12	3	✗	✗	✓
Water-pouring	7	6	✗	✗	✗
Insert-T	52	2	✓	✓	✗

action $\boldsymbol{a}^r$ and state $\boldsymbol{s}$. Then, the human model is trained by minimizing the loss $\ell_H = \min_\phi \|H_\phi(\boldsymbol{a}^r, \boldsymbol{s}) - \boldsymbol{h}\|^2$, and the policy model is trained by minimizing the loss

$$\ell_\pi^{\text{BD-COACH}}(\boldsymbol{s}) = \min_{\boldsymbol{\theta}} \|\boldsymbol{\mu}_{\boldsymbol{\theta}}(\boldsymbol{s}) - \hat{\boldsymbol{a}}^h\|^2,$$

where $\hat{\boldsymbol{a}}^h = \boldsymbol{a}^r + e \cdot H_\phi(\boldsymbol{a}^r, \boldsymbol{s})$. Therefore, since $\hat{\boldsymbol{a}}^h$ is estimated in relation to the current robot's policy, the correction data is no longer outdated.

2) HG-DAgger: HG-DAgger is an intervention-based IIL algorithm that aggregates human demonstrations into a dataset and updates its behavior at the end of each episode by minimizing the distance between its current policy and the actions stored in the dataset. In contrast, methods like CLIC and D-COACH update the policy continuously during training episodes, as shown in Algorithm 1 (line 9). To make a fair comparison and make the IIL framework consistent across different methods, we introduce a slight modification to HG-DAgger, allowing it to update its policy during each training episode, similar to CLIC. This modification enables HG-DAgger to converge faster than its original version.

HG-DAgger assumes an explicit Gaussian policy and updates it using behavior cloning loss (see Eq. (22)). For other offline BC baselines, such as Diffusion Policy and IBC, we adopt the HG-DAgger framework while replacing only the policy update step with their respective methods.

E. The Setup of Experiments

In all the experiments, we used state-based observation as input for the policy across all methods. The summary of the tasks in both the simulation and the real world is reported in Table V. The term 'multi-modal' denotes whether the task has multiple solutions inside the dataset.

1) Simulated tasks: The task descriptions are as follows:

i) **Push-T:** This task, introduced by [6], involves the robot pushing a T-shape object to a fixed target using its circular end effector.

ii) **Square:** The robot must place a square-shaped nut onto a fixed square peg.

iii) **Pick-Can:** The objective is to pick up a can object and transport it to a fixed target bin.

iv) **TwoArm-Lift:** This task involves two robots working together to lift a shared object.

For each task, the object's position is randomly initialized at the beginning of each episode.

2) Real-world tasks: The learned policy is evaluated every 5 episodes for the water-pouring task, every 10 episodes for the ball-catching task, and every 20 episodes for the Insert-T task. The details of each real-world task are detailed as follows:

i) **Ball catching:** This task involves the robot catching a ball that's swinging on a string attached to a fixed point. The robot's end effector operates within the same plane where the ball swings, maintaining a fixed orientation. The action space consists of the robot's end effector linear velocity in the specified plane and a one-dimensional continuous actuation command for controlling the robot's gripper, where 0 represents fully closed and 1 fully open. The state space includes the end-effector's relative position and velocity with respect to the ball, the angle between the gravity vector and the ball's string along with its corresponding angular velocity, and the poses of both the ball and the fixed point. The poses of the ball and the fixed point are measured using an OptiTrack system.

ii) **Water pouring:** The robot controls the pose of a bottle to precisely pour liquid (represented with marbles) into a small bowl. The action space is 6D, consisting of the robot's end-effector linear and angular velocities. The state space is defined by the robot's end-effector pose, which consists of its Cartesian position and its orientation, represented with a unit quaternion. The initial pose of the robot is randomized at the start of each episode within certain position and orientation limits to ensure safety.

iii) **Insert-T:** The robot must insert a T-shape object into a U-shape object by pushing them. The action space is defined as the linear velocity of the end-effector in a 2D plane over the table. The robot's end-effector orientation and z-axis position (the one aligned with the table's normal vector) are fixed throughout the task. The positions of the objects are measured by an OptiTrack system. The state space consists of the positions of 10 key points on a T-shape object, the positions of 10 key points on a U-shape object, and the position and velocity of the end-effector.

3) Time duration: The total time duration of the real-world experiments within the IIL framework is reported in Table VI, excluding the time spent resetting the robot or performing evaluations.

TABLE VI: Total time duration of real-world experiments

	Ball-catching	Water-pouring	Insert-T
Time duration (minutes)	74	40	140

F. Time Efficiency Comparison

TABLE VII: Time efficiency comparison per step

	CLIC-Half	CLIC-Circular	CLIC-Explicit
Inference time (ms)	28.61	28.52	1.13
Training time (ms)	201.32	176.64	12.66

For all CLIC methods with a batch size of 32, the inference and training times per step on the Square task were recorded and averaged. As reported in Table VII, although implicit models have better encoding capability, they require more time for both training and inference compared to the explicit model used in CLIC-Explicit. This presents a trade-off when selecting

an algorithm for practical use. For uni-modal tasks, CLIC-Explicit can be used for its time efficiency. For multi-modal tasks, CLIC-Half and CLIC-Circular should be used instead. Additionally, Table VII shows that CLIC-Half has a slightly longer training time per step than CLIC-Circular, as it involves an additional step of sampling implicit negative actions.

G. Implementation Details

1) Network structure: For implicit policies, CLIC, IBC, and PVP use the same neural network structure for the EBM. The neural network consists of five fully connected layers with [512, 512, 512, 256, 1] units, respectively. The ReLU activation function is applied between all layers except for the last layer, which has no activation function. The input is the concatenation of the state and action vectors, and the output is a scalar. For Diffusion Policy, the neural network follows a similar structure, except that the last layer has a number of units equal to the dimensionality of the action space.

For the explicit policy $\pi_{\boldsymbol{\theta}}(\boldsymbol{s}, \boldsymbol{a}) \sim \mathcal{N}(\boldsymbol{\mu}_{\boldsymbol{\theta}}(\boldsymbol{s}), \boldsymbol{\Sigma})$, the mean $\boldsymbol{\mu}_{\boldsymbol{\theta}}(\boldsymbol{s})$ is parameterized by a neural network consisting of five fully connected layers. The layer units are the same as the Diffusion Policy's model; except that the final layer applies a sigmoid activation, followed by scaling and shifting to produce values between -1 and 1. This neural network takes a state vector as input and maps it to an action. This action is obtained via $\boldsymbol{a}_t = \boldsymbol{\mu}_{\boldsymbol{\theta}}(\boldsymbol{s}_t)$. The covariance matrix $\boldsymbol{\Sigma}$ can be chosen to control the variability of actions sampled from the Gaussian distribution. In our implementation, it is ignored entirely, in which case actions are always taken as $\boldsymbol{\mu}_{\boldsymbol{\theta}}(\boldsymbol{s}_t)$.

2) Gradient Penalty: As described in Appendix B.3.1 of IBC [1], we incorporate a gradient penalty loss to improve the training stability of CLIC. This penalty is computed using only the action samples from the final MCMC step. In practice, we found that the gradient penalty used in IBC is more effective than the L2 norm penalty.

3) Hyperparameters for Training: At each training episode, the network parameters will be updated with an update frequency of $b = 5$ for all methods, as shown in line 6 of Algorithm 1. The batch size is set to 32 for accurate, relative, and partial feedback, and 10 for noisy feedback. The learning rate is 0.003. The optimizer for the neural network is Adam with $\beta_1 = 0.1, \beta_2 = 0.999$ and $\epsilon = 1e - 7$. The number of training steps at the end of each episode, $N_{training}$, is set to 500 for all methods except diffusion policy, for which it is set to 1000.

For CLIC-Circular, ε is set to 0.5, and the temperature T is set to 0.05 for all tasks. For CLIC-Half, the hyperparameters α and ε are set to $\alpha = 30°$ and $\varepsilon = 0.3$ for accurate and relative feedback; and set to $100°$ and $\varepsilon = 0.1$ for partial and noisy feedback. For the Insert-T task, $\alpha = 30°$ and $\varepsilon = 0.1$. The number of implicit negative actions, N_I, is 128. The magnitude hyperparameter is $e = 0.2$. The number of sampled actions from EBM is $N_a = 512$. $N_{\text{MCMC}} = 25$ during training and $N_{\text{MCMC}} = 50$ during inference.

For IBC, $N_{\text{neg}} = 512$, $N_{\text{MCMC}} = 25$ during training and $N_{\text{MCMC}} = 50$ during inference.

REFERENCES

[1] P. Florence, C. Lynch, A. Zeng, O. A. Ramirez, A. Wahid, L. Downs, A. Wong, J. Lee, I. Mordatch, and J. Tompson, "Implicit behavioral cloning," in *Conf. on Robot Learn.*, pp. 158–168, PMLR, 2022.

[2] T. Osa, J. Pajarinen, G. Neumann, J. A. Bagnell, P. Abbeel, J. Peters, *et al.*, "An algorithmic perspective on imitation learning," *Found. Trends Robotics*, vol. 7, no. 1-2, pp. 1–179, 2018.

[3] H. Ravichandar, A. S. Polydoros, S. Chernova, and A. Billard, "Recent advances in robot learning from demonstration," *Annu. Review Control. Robotics, Auton. Syst.*, vol. 3, no. 1, pp. 297–330, 2020.

[4] M. Zare, P. M. Kebria, A. Khosravi, and S. Nahavandi, "A survey of imitation learning: Algorithms, recent developments, and challenges," *IEEE Trans. on Cybern.*, 2024.

[5] S. Habibian, A. A. Valdivia, L. H. Blumenschein, and D. P. Losey, "A survey of communicating robot learning during human-robot interaction," *The Int. J. Robotics Research*, vol. 0, no. 0, p. 02783649241281369, 0.

[6] C. Chi, S. Feng, Y. Du, Z. Xu, E. Cousineau, B. Burchfiel, and S. Song, "Diffusion policy: Visuomotor policy learning via action diffusion," in *Proc. Robotics: Sci. Syst. (RSS)*, 2023.

[7] D.-N. Ta, E. Cousineau, H. Zhao, and S. Feng, "Conditional energy-based models for implicit policies: The gap between theory and practice," *arXiv preprint arXiv:2207.05824*, 2022.

[8] M. Reuss, M. Li, X. Jia, and R. Lioutikov, "Goal conditioned imitation learning using score-based diffusion policies," in *Robotics: Sci. Syst.*, 2023.

[9] H. Ding, N. Jaquier, J. Peters, and L. Rozo, "Fast and robust visuomotor riemannian flow matching policy," *arXiv preprint arXiv:2412.10855*, 2024.

[10] J. Urain, A. Mandlekar, Y. Du, M. Shafiullah, D. Xu, K. Fragkiadaki, G. Chalvatzaki, and J. Peters, "Deep generative models in robotics: A survey on learning from multimodal demonstrations," *arXiv preprint arXiv:2408.04380*, 2024.

[11] C. Celemin, R. Pérez-Dattari, E. Chisari, G. Franzese, L. de Souza Rosa, R. Prakash, Z. Ajanović, M. Ferraz, A. Valada, J. Kober, *et al.*, "Interactive imitation learning in robotics: A survey," *Found. Trends Robotics*, vol. 10, no. 1-2, pp. 1–197, 2022.

[12] C. Celemin, G. Maeda, J. Ruiz-del Solar, J. Peters, and J. Kober, "Reinforcement learning of motor skills using policy search and human corrective advice," *The Int. J. Robotics Research*, vol. 38, no. 14, pp. 1560–1580, 2019.

[13] R. Pérez-Dattari, C. Celemin, J. Ruiz-del Solar, and J. Kober, "Continuous control for high-dimensional state spaces: An interactive learning approach," in *2019 Int. Conf. on Robotics Autom. (ICRA)*, pp. 7611–7617, IEEE, 2019.

[14] C. Celemin and J. Ruiz-del Solar, "An interactive framework for learning continuous actions policies based on corrective feedback," *J. Intell. & Robotic Syst.*, vol. 95, pp. 77–97, 2019.

[15] Y. Du and I. Mordatch, "Implicit generation and modeling with energy based models," in *Adv. Neural Inf. Process. Syst.*, vol. 32, 2019.

[16] B. P. Graesdal, S. Y. C. Chia, T. Marcucci, S. Morozov, A. Amice, P. A. Parrilo, and R. Tedrake, "Towards tight convex relaxations for contact-rich manipulation," in *Proc. Robotics: Sci. Syst. (RSS)*, 2024.

[17] Y. Song and D. P. Kingma, "How to train your energy-based models," *arXiv preprint arXiv:2101.03288*, 2021.

[18] J. Sohl-Dickstein, E. Weiss, N. Maheswaranathan, and S. Ganguli, "Deep unsupervised learning using nonequilibrium thermodynamics," in *Int. Conf. on Mach. Learn.*, pp. 2256–2265, PMLR, 2015.

[19] J. Ho, A. Jain, and P. Abbeel, "Denoising diffusion probabilistic models," in *Adv. Neural Inf. Process. Syst.*, vol. 33, pp. 6840–6851, 2020.

[20] Y. Song, J. Sohl-Dickstein, D. P. Kingma, A. Kumar, S. Ermon, and B. Poole, "Score-based generative modeling through stochastic differential equations," in *Int. Conf. on Learn. Represent.*, 2021.

[21] J. Jankowski, A. Maric, P. Liu, D. Tateo, J. Peters, and S. Calinon, "Energy-based contact planning under uncertainty for robot air hockey," *CoRR*, 2024.

[22] Z. Zhang, J. Hong, A. M. S. Enayati, and H. Najjaran, "Using implicit behavior cloning and dynamic movement primitive to facilitate reinforcement learning for robot motion planning," *IEEE Trans. on Robotics*, 2024.

[23] G. Datta, R. Hoque, A. Gu, E. Solowjow, and K. Goldberg, "Iifl: Implicit interactive fleet learning from heterogeneous human supervisors," in *Conf. on Robot Learn.*, pp. 2340–2356, PMLR, 2023.

[24] S.-W. Lee and Y.-L. Kuo, "Diff-dagger: Uncertainty estimation with diffusion policy for robotic manipulation," *arXiv preprint arXiv:2410.14868*, 2024.

[25] P. F. Christiano, J. Leike, T. Brown, M. Martic, S. Legg, and D. Amodei, "Deep reinforcement learning from human preferences," in *Adv. Neural Inf. Process. Syst.*, vol. 30, 2017.

[26] A. Jain, S. Sharma, T. Joachims, and A. Saxena, "Learning preferences for manipulation tasks from online coactive feedback," *The Int. J. Robotics Research*, vol. 34, no. 10, pp. 1296–1313, 2015.

[27] K. Lee, L. M. Smith, and P. Abbeel, "Pebble: Feedback-efficient interactive reinforcement learning via relabeling experience and unsupervised pre-training," in *Int. Conf. on Mach. Learn.*, pp. 6152–6163, PMLR, 2021.

[28] N. Stiennon, L. Ouyang, J. Wu, D. Ziegler, R. Lowe, C. Voss, A. Radford, D. Amodei, and P. F. Christiano, "Learning to summarize with human feedback," in *Adv. Neural Inf. Process. Syst.*, vol. 33, pp. 3008–3021, 2020.

[29] Z. Yang, M. Jun, J. Tien, S. Russell, A. Dragan, and E. Biyik, "Trajectory improvement and reward learning from comparative language feedback," in *8th Annu. Conf. on Robot Learn.*, 2024.

[30] J. Hejna, R. Rafailov, H. Sikchi, C. Finn, S. Niekum, W. B. Knox, and D. Sadigh, "Contrastive preference learning: Learning from human feedback without reinforcement learning," in *The Twelfth Int. Conf. on Learn. Represent.*, 2024.

[31] Y. Zhao, M. Khalman, R. Joshi, S. Narayan, M. Saleh, and P. J. Liu, "Calibrating sequence likelihood improves conditional language generation," in *The Eleventh Int. Conf. on Learn. Represent.*, 2022.

[32] R. Rafailov, A. Sharma, E. Mitchell, C. D. Manning, S. Ermon, and C. Finn, "Direct preference optimization: Your language model is secretly a reward model," in *Adv. Neural Inf. Process. Syst.*, vol. 36, 2024.

[33] D. Brown, W. Goo, P. Nagarajan, and S. Niekum, "Extrapolating beyond suboptimal demonstrations via inverse reinforcement learning from observations," in *Int. Conf. on Mach. Learn.*, pp. 783–792, PMLR, 2019.

[34] E. Biyik, N. Anari, and D. Sadigh, "Batch active learning of reward functions from human preferences," *ACM Trans. on Human-Robot Interact.*, vol. 13, no. 2, pp. 1–27, 2024.

[35] M. Verma and K. Metcalf, "Hindsight PRIORs for reward learning from human preferences," in *The Twelfth Int. Conf. on Learn. Represent.*, 2024.

[36] A. Bajcsy, D. P. Losey, M. K. O'malley, and A. D. Dragan, "Learning robot objectives from physical human interaction," in *Conf. on Robot Learn.*, pp. 217–226, PMLR, 2017.

[37] D. P. Losey and M. K. O'Malley, "Including uncertainty when learning from human corrections," in *Conf. on Robot Learn.*, pp. 123–132, PMLR, 2018.

[38] W. Jin, T. D. Murphey, Z. Lu, and S. Mou, "Learning from human directional corrections," *IEEE Trans. on Robotics*, vol. 39, no. 1, pp. 625–644, 2022.

[39] R. Pérez-Dattari, C. Celemin, J. Ruiz-del Solar, and J. Kober, "Interactive learning with corrective feedback for policies based on deep neural networks," in *Proc. 2018 Int. Symp. on Exp. Robotics*, pp. 353–363, Springer, 2020.

[40] I. Lopez Bosque, "Towards corrective deep imitation learning in data intensive environments: Helping robots to learn faster by leveraging human knowledge," master's thesis, Delft University of Technology, Nov. 2021.

[41] S. Jauhri, C. Celemin, and J. Kober, "Interactive imitation learning in state-space," in *Conf. on Robot Learn.*, pp. 682–692, PMLR, 2021.

[42] Z. Peng, W. Mo, C. Duan, Q. Li, and B. Zhou, "Learning from active human involvement through proxy value propagation," in *Adv. Neural Inf. Process. Syst.*, 2023.

[43] T. Haarnoja, H. Tang, P. Abbeel, and S. Levine, "Reinforcement learning with deep energy-based policies," in *Int. Conf. on Mach. Learn.*, pp. 1352–1361, PMLR, 2017.

[44] T. Haarnoja, A. Zhou, P. Abbeel, and S. Levine, "Soft actor-critic: Off-policy maximum entropy deep reinforcement learning with a stochastic actor," in *Int. Conf. on Mach. Learn.*, pp. 1861–1870, PMLR, 2018.

[45] X. Bu, W. Li, Z. Liu, Z. Ma, and P. Huang, "Aligning human intent from imperfect demonstrations with confidence-based inverse soft-q learning," *IEEE Robotics Autom. Lett.*, 2024.

[46] W. Ding, T. Che, D. Zhao, and M. Pavone, "Bayesian reparameterization of reward-conditioned reinforcement learning with energy-based models," in *Int. Conf. on Mach. Learn.*, pp. 8053–8066, PMLR, 2023.

[47] J. Hejna and D. Sadigh, "Inverse preference learning: Preference-based rl without a reward function," in *Adv. Neural Inf. Process. Syst.*, vol. 36, 2024.

[48] J. Spencer, S. Choudhury, M. Barnes, M. Schmittle, M. Chiang, P. Ramadge, and S. Srinivasa, "Learning from interventions: Human-robot interaction as both explicit and implicit feedback," in *16th Robotics: Sci. Syst. RSS 2020*, MIT Press Journals, 2020.

[49] R. Gao, E. Nijkamp, D. P. Kingma, Z. Xu, A. M. Dai, and Y. N. Wu, "Flow contrastive estimation of energy-based models," in *Proc. IEEE/CVF Conf. on Comput. Vis. Pattern Recognit.*, pp. 7518–7528, 2020.

[50] Y. Kalantidis, M. B. Sariyildiz, N. Pion, P. Weinzaepfel, and D. Larlus, "Hard negative mixing for contrastive learning," in *Adv. Neural Inf. Process. Syst.*, vol. 33, pp. 21798–21809, 2020.

[51] S. Ross, G. Gordon, and D. Bagnell, "A reduction of imitation learning and structured prediction to no-regret online learning," in *Proc. Fourteenth Int. Conf. on Artif. Intell. Stat.*, pp. 627–635, JMLR Workshop and Conference Proceedings, 2011.

[52] A. v. d. Oord, Y. Li, and O. Vinyals, "Representation learning with contrastive predictive coding," *arXiv preprint arXiv:1807.03748*, 2018.

[53] S. Singh, S. Tu, and V. Sindhwani, "Revisiting energy based models as policies: Ranking noise contrastive estimation and interpolating energy models," *Trans. on Mach. Learn. Research*, 2024.

[54] M. Welling and Y. W. Teh, "Bayesian learning via stochastic gradient langevin dynamics," in *Proc. 28th Int. Conf. on Mach. Learn. (ICML-11)*, pp. 681–688, Citeseer, 2011.

[55] M. Kelly, C. Sidrane, K. Driggs-Campbell, and M. J. Kochenderfer, "Hg-dagger: Interactive imitation learning with human experts," in *2019 Int. Conf. on Robotics Autom. (ICRA)*, pp. 8077–8083, IEEE, 2019.

[56] Y. Zhu, J. Wong, A. Mandlekar, R. Martín-Martín, A. Joshi, S. Nasiriany, and Y. Zhu, "robosuite: A modular simulation framework and benchmark for robot learning," in *arXiv preprint arXiv:2009.12293*, 2020.

[57] R. Pérez-Dattari, C. Celemin, G. Franzese, J. Ruiz-del Solar, and J. Kober, "Interactive learning of temporal features for control: Shaping policies and state representations from human feedback," *IEEE Robotics & Autom. Mag.*, vol. 27, no. 2, pp. 46–54, 2020.